Short Article

Cell Stem Cell

Targeting the RNA m^{6}A Reader YTHDF2 Selectively Compromises Cancer Stem Cells in Acute Myeloid Leukemia

Graphical Abstract

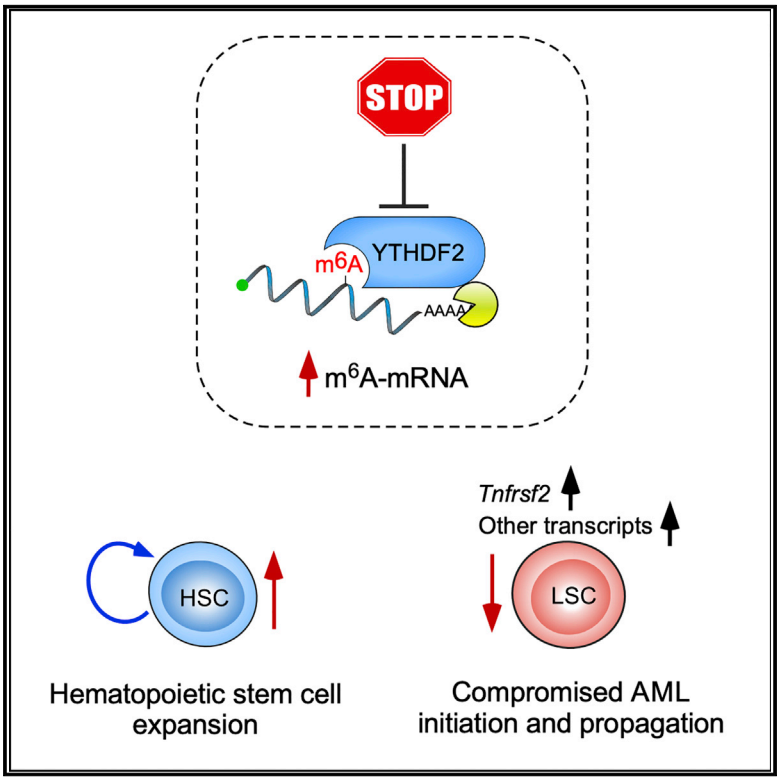

Authors

Jasmin Paris, Marcos Morgan, Joana Campos, ..., Richard I. Gregory, Dónal O'Carroll, Kamil R. Kranc

Correspondence

donal.ocarroll@ed.ac.uk (D.O.), kamil.kranc@qmul.ac.uk (K.R.K.)

In Brief

Elimination of cancer stem cells in acute myeloid leukemia (AML) while preserving hematopoiesis is a challenge in leukemia treatment. Paris et al. demonstrate that inactivation of the RNA m^{6}A reader YTHDF2 increases the half-life of m^{6}A-modified transcripts and specifically compromises cancer stem cells, highlighting YTHDF2 as an essential regulator of AML.

Highlights

- YTHDF2 is highly expressed across human AML and is essential for leukemia initiation
- YTHDF2 shortens the half-life of m^{6}A-modified transcripts in AML
- Loss of YTHDF2 expands HSCs but does not derail hematopoiesis
- YTHDF2 protects AML cells from apoptosis by downregulating TNFR2

Paris et al., 2019, Cell Stem Cell *25*, 137–148
July 3, 2019
https://doi.org/10.1016/j.stem.2019.03.021

CellPress

Cell Stem Cell
Short Article

Targeting the RNA m^{6}A Reader YTHDF2 Selectively Compromises Cancer Stem Cells in Acute Myeloid Leukemia

Jasmin Paris,[1,2,9] Marcos Morgan,[1,3,4,9] Joana Campos,[1,2,9] Gary J. Spencer,[5] Alena Shmakova,[1] Ivayla Ivanova,[1,3] Christopher Mapperley,[1] Hannah Lawson,[1,2] David A. Wotherspoon,[1,2] Catarina Sepulveda,[1] Milica Vukovic,[1] Lewis Allen,[1] Annika Sarapuu,[1,2] Andrea Tavosanis,[2] Amelie V. Guitart,[1] Arnaud Villacreces,[1] Christian Much,[1,3] Junho Choe,[6] Ali Azar,[1,2] Louie N. van de Lagemaat,[1,2] Douglas Vernimmen,[7] Ali Nehme,[8] Frederic Mazurier,[8] Tim C.P. Somervaille,[5] Richard I. Gregory,[6] Dónal O'Carroll,[1,3,4,10,*] and Kamil R. Kranc[1,2,10,11,*]
[1]MRC Centre for Regenerative Medicine, University of Edinburgh, Edinburgh EH16 4UU, UK
[2]Laboratory of Haematopoietic Stem Cell & Leukaemia Biology, Centre for Haemato-Oncology, Barts Cancer Institute, Queen Mary University of London, London EC1M 6BQ, UK
[3]Institute for Stem Cell Research, School of Biological Sciences, University of Edinburgh, Edinburgh EH16 4UU, UK
[4]Wellcome Centre for Cell Biology, School of Biological Sciences, University of Edinburgh, Edinburgh EH9 3BF, UK
[5]Leukaemia Biology Laboratory, Cancer Research UK Manchester Institute, University of Manchester, Manchester M20 4GJ, UK
[6]Department of Biological Chemistry and Molecular Pharmacology, Harvard Medical School, Boston, MA, USA
[7]Roslin Institute, University of Edinburgh, Edinburgh EH25 9RG, UK
[8]Université de Tours, CNRS, LNOx ERL 7001, Tours, France
[9]These authors contributed equally
[10]These authors contributed equally
[11]Lead Contact
*Correspondence: donal.ocarroll@ed.ac.uk (D.O.), kamil.kranc@qmul.ac.uk (K.R.K.)
https://doi.org/10.1016/j.stem.2019.03.021

SUMMARY

Acute myeloid leukemia (AML) is an aggressive clonal disorder of hematopoietic stem cells (HSCs) and primitive progenitors that blocks their myeloid differentiation, generating self-renewing leukemic stem cells (LSCs). Here, we show that the mRNA m^{6}A reader YTHDF2 is overexpressed in a broad spectrum of human AML and is required for disease initiation as well as propagation in mouse and human AML. YTHDF2 decreases the half-life of diverse m^{6}A transcripts that contribute to the overall integrity of LSC function, including the tumor necrosis factor receptor *Tnfrsf2*, whose upregulation in *Ythdf2*-deficient LSCs primes cells for apoptosis. Intriguingly, YTHDF2 is not essential for normal HSC function, with YTHDF2 deficiency actually enhancing HSC activity. Thus, we identify YTHDF2 as a unique therapeutic target whose inhibition selectively targets LSCs while promoting HSC expansion.

INTRODUCTION

Hematopoiesis critically depends on hematopoietic stem cells (HSCs), which possess unique self-renewal capacity and multilineage differentiation potential, replenishing all blood lineages (Orkin and Zon, 2008). Acute myeloid leukemia (AML) is an aggressive clonal disorder of hematopoietic stem and progenitor cells (HSPCs) in which the acquisition of mutations by HSPCs results in a block in their myeloid differentiation and the generation of self-renewing leukemic stem cells (LSCs) (Döhner et al., 2015). LSCs initiate and propagate the disease, and given that they are treatment resistant, they often fuel disease relapses. Therefore, identification of specific therapeutic targets for LSC elimination is an unmet clinical need.

Emerging evidence indicates an involvement of mRNA N6-methyladenosine (m^{6}A) modification, the most abundant internal mRNA modification (Desrosiers et al., 1974; Perry and Kelley, 1974), in hematopoietic specification, differentiation, and pathogenesis of AML (Barbieri et al., 2017; Li et al., 2017; Vu et al., 2017; Weng et al., 2018; Zhang et al., 2017). The m^{6}A modification is deposited by the m^{6}A methyltransferase complex (m^{6}A writer) composed of a METTL3 and METTL14 heterodimeric enzymatic core and their regulator, WTAP (Bokar et al., 1997; Liu et al., 2014; Ping et al., 2014; Tuck, 1992; Wang et al., 2014b), and reversed by m^{6}A demethylases (FTO and AlkBH5; Jia et al., 2011; Zheng et al., 2013) referred to as m^{6}A erasers. Recent studies revealed the requirement for METTL3, METTL14, and FTO in leukemic transformation and established the importance of m^{6}A modification in AML (Barbieri et al., 2017; Li et al., 2017; Vu et al., 2017; Weng et al., 2018). However, while m^{6}A modification regulates mRNA processing, translation, and degradation (Fu et al., 2014), the functional contributions of these m^{6}A-dependent processes to leukemic transformation have not been explored.

The outcome of RNA m^{6}A modification is executed by the YTH (YT521-B homology) domain proteins (known as readers), including nuclear YTHDC1 (Xiao et al., 2016a; Xu et al., 2014) and cytoplasmic YTHDF1–YTHDF3 and YTHDC2 (Shi et al., 2017; Tanabe et al., 2016; Wang et al., 2014a, 2015). Nuclear YTHDC1 regulates mRNA splicing and nuclear export (Xiao

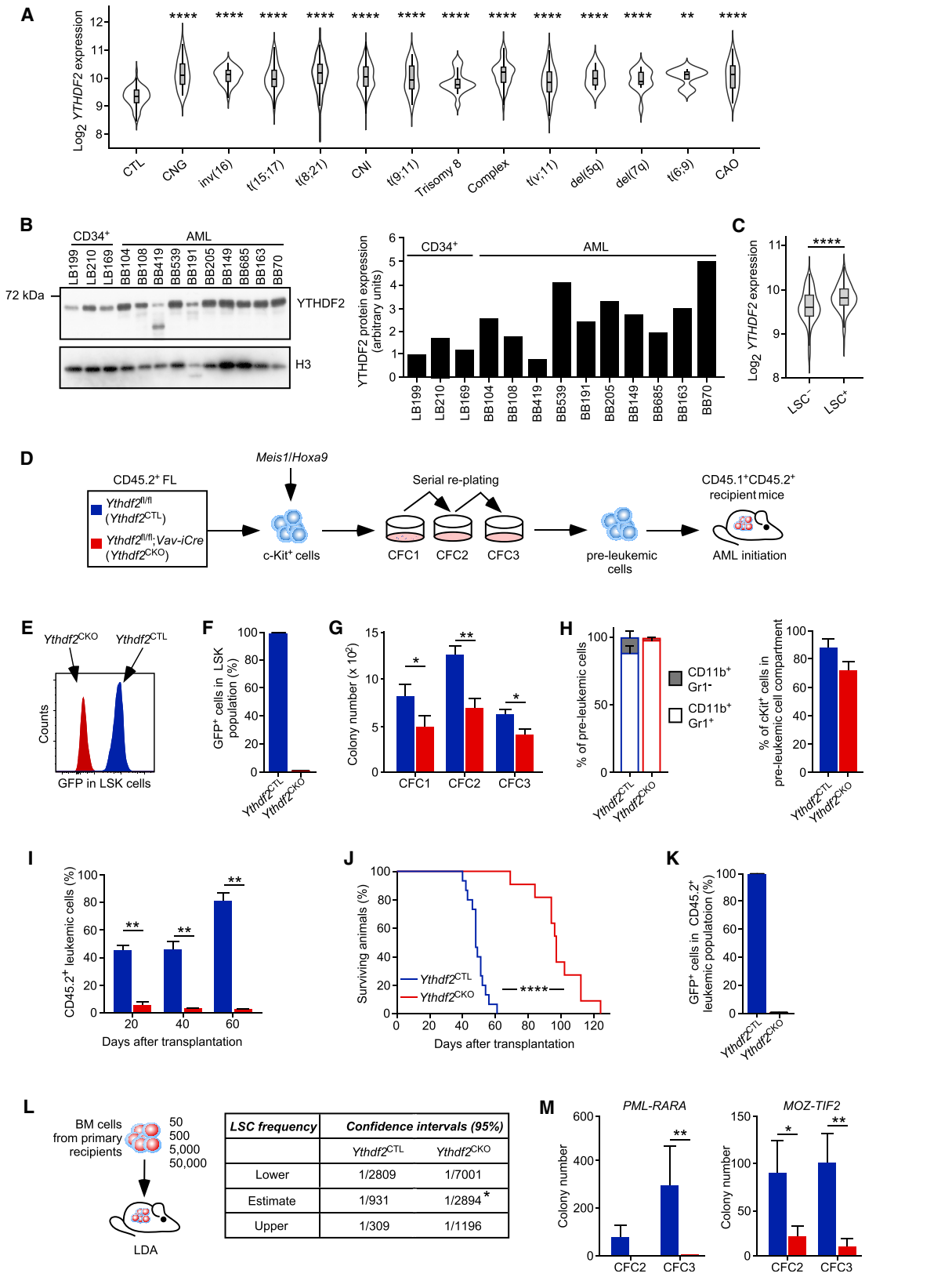

LSC frequency	Confidence intervals (95%)	
	Ythdf2^{CTL}	*Ythdf2*^{CKO}
Lower	1/2809	1/7001
Estimate	1/931	1/2894 *
Upper	1/309	1/1196

(legend on next page)

et al., 2016a). While YTHDF1 and YTHDF3 binding to m^{6}A enhances mRNA translation (Shi et al., 2017; Wang et al., 2015), YTHDF2 recognizes m^{6}A mRNA within the GACU/A consensus to mediate degradation of m^{6}A transcripts (Du et al., 2016; Wang et al., 2015). Although previous studies perturbing the whole m^{6}A pathway have established its significance in AML pathogenesis (Barbieri et al., 2017; Li et al., 2017; Vu et al., 2017; Weng et al., 2018), the functions of specific m^{6}A readers in leukemia remain unexplored. However, recent studies implicated *Ythdf2* in the regulation of HSC homeostasis and hematopoietic regeneration (Li et al., 2018; Wang et al., 2018). Here, we reveal that targeting YTHDF2 extends the half-life of m^{6}A-modified transcripts to selectively compromise AML initiation and propagation without derailing normal hematopoiesis.

RESULTS

Ythdf2 Is Essential for LSC Development and AML Initiation

We found that *YTHDF2* was expressed significantly higher across AML samples with diverse cytogenetic abnormalities compared to non-leukemic controls (Figure 1A), and YTHDF2 protein was highly expressed in primary AML samples (Figure 1B). We next compared *YTHDF2* expression in datasets from AML cells with LSC activity and AML cells without LSC activity validated by xenotransplantation (Ng et al., 2016) and found that *YTHDF2* expression correlated with LSC activity (Figure 1C). Given that the majority of CD34$^+$ and a minority of CD34$^-$ fractions have LSC activity (Eppert et al., 2011; Sarry et al., 2011), we also compared *YTHDF2* expression between these fractions and found that *YTHDF2* was expressed at higher levels in CD34$^+$ fractions (Figure S1A). To investigate the requirement for YTHDF2 in leukemogenesis, we employed conditional genetics and a mouse AML model in which *Meis1* and *Hoxa9*, oncogenes frequently overexpressed in human AML (Drabkin et al., 2002; Lawrence et al., 1999), drive leukemogenesis. In this model (Figure 1D), HSPCs are transduced with retroviruses co-expressing *Meis1* and *Hoxa9* and serially replated, generating preleukemic cells, which upon transplantation to recipient mice generate self-renewing LSCs, causing AML (Guitart et al., 2017; Kroon et al., 1998; Vukovic et al., 2015). We utilized the conditional and reporter *Ythdf2*^{fl} mouse allele in which exon 2 of *Ythdf2* was flanked by *loxP* sites and GFP was inserted after the start codon of *Ythdf2* in exon 1, generating a fully functional GFP-YTHDF2 fusion protein (Ivanova et al., 2017). We combined the *Ythdf2*^{fl} allele with *Vav-iCre* (de Boer et al., 2003) to generate *Ythdf2*$^{fl/fl}$;*Vav-iCre* (*Ythdf2*^{CKO}) mice in which *Ythdf2* is specifically deleted in the hematopoietic system shortly after the emergence of HSCs (Figures 1E and 1F). *Ythdf2*^{CKO} and control *Ythdf2*$^{fl/fl}$ (*Ythdf2*^{CTL}) mice showed normal Mendelian distribution (*Ythdf2*$^{fl/fl}$ × *Ythdf2*$^{fl/fl}$;*Vav-iCre* matings resulted in 65 *Ythdf2*^{CTL} and 47 *Ythdf2*^{CKO} mice at weaning; p = 0.28) and had comparable survival. We transduced *Ythdf2*^{CKO} and *Ythdf2*^{CTL} HSPCs with *Meis1-Hoxa9* retroviruses and found that while *Ythdf2*^{CKO} cells produced significantly lower colony numbers upon serial replating (Figure 1G), they had unaffected expression of c-Kit, CD11b, and Gr-1 (Figure 1H). Notably, *Ythdf2*-deficient preleukemic cells generated AML with substantially longer latency compared to control cells (Figures 1I and 1J). The loss of YTHDF2 expression was confirmed in *Ythdf2*^{CKO} cells isolated from moribund recipient mice (Figure 1K). To enumerate LSCs in the leukemic recipients of *Meis1-Hoxa9*-transduced *Ythdf2*^{CKO} and *Ythdf2*^{CTL} cells, we performed a limiting dilution assay with donor-derived CD45.2$^+$ bone marrow (BM) cells isolated from primary recipients. We found that LSC frequency in recipients of *Ythdf2*^{CKO} cells was significantly decreased (Figure 1L). Therefore, *Ythdf2* is required for LSC development and AML initiation.

To test whether *Ythdf2* is required for leukemic transformation driven by other oncogenes, we used PML-RARA, which causes acute promyelocytic leukemia, and MOZ-TIF2, which is associated with AML with inv(8)(p11q13). Serial replating assays revealed that *Ythdf2*^{CKO} c-Kit$^+$ cells transduced with either PML-RARA or MOZ-TIF2 retroviruses failed to efficiently generate colonies (Figure 1M). Thus, *Ythdf2* is essential for leukemic transformation driven also by other oncogenes.

Figure 1. *YTHDF2* Is Upregulated in Different AML Subtypes and Is Essential for AML Development

(A) *YTHDF2* gene expression in control (CTL) and different cytogenetic subgroups of human AML bone marrow samples. Violin plots show the distribution of $\log_2$ expression values. Horizontal line in the boxplots indicates median. CNG, cytologically normal with good prognosis; CNI, cytologically normal with intermediate prognosis; CAO, cytologically abnormal not otherwise specified.

(B) Western blot of YTHDF2 in normal human CD34$^+$ cells and AML samples (karyotype details are shown in STAR Methods) (left). α-Histone 3 (H3) was used as a loading control. Quantification of YTHDF2 normalized to H3 expression is presented (right).

(C) *YTHDF2* gene expression in primitive AML cell compartments with (LSC$^+$) and without (LSC$^-$) leukemic engraftment potential.

(D) Control *Ythdf2*$^{fl/fl}$ (*Ythdf2*^{CTL}) and *Ythdf2*$^{fl/fl}$;*Vav-iCre* (*Ythdf2*^{CKO}) fetal liver (FL) c-Kit$^+$ cells were co-transduced with *Meis1* and *Hoxa9* retroviruses and serially replated. c-Kit$^+$ preleukemic cells were transplanted into recipient mice (n = 12–14).

(E) A representative histogram showing GFP-YTHDF2 protein expression in *Ythdf2*^{CTL} FL LSK cells and the lack of GFP-YTHDF2 expression in *Ythdf2*^{CKO} FL LSK cells.

(F) Percentage of GFP-positive cells in the 14.5 days post coitum (dpc) FL LSK cell population from FLs of *Ythdf2*^{CTL} and *Ythdf2*^{CKO} embryos (n = 5).

(G) CFC counts at each replating (n = 3).

(H) Percentage of CD11b$^+$Gr-1$^-$, CD11b$^+$Gr-1$^+$, and c-Kit$^+$ cells in the preleukemic cell compartment (n = 4–5).

(I) Percentage of CD45.2$^+$ leukemic cells in the PB of recipient mice (n = 12–14 per genotype).

(J) Survival curve of recipients transplanted with preleukemic cells (n = 12–14).

(K) Percentage of GFP-positive cells in the CD45.2$^+$ cell population from moribund recipients of *Ythdf2*^{CTL} and *Ythdf2*^{CKO} cells (n = 5–6).

(L) Limiting dilution assay (LDA). Secondary recipients (n = 5–8) were transplanted with indicated doses of CD45.2$^+$ BM cells from primary recipients.

(M) *Ythdf2*^{CTL} and *Ythdf2*^{CKO} FL c-Kit$^+$ cells were transduced with *MOZ-TIF2* or *PML-RARA* retroviruses and serially replated. CFC counts at each replating are shown (n = 3).

Data represent mean ± SEM; *p < 0.05; **p < 0.01; ****p < 0.0001.

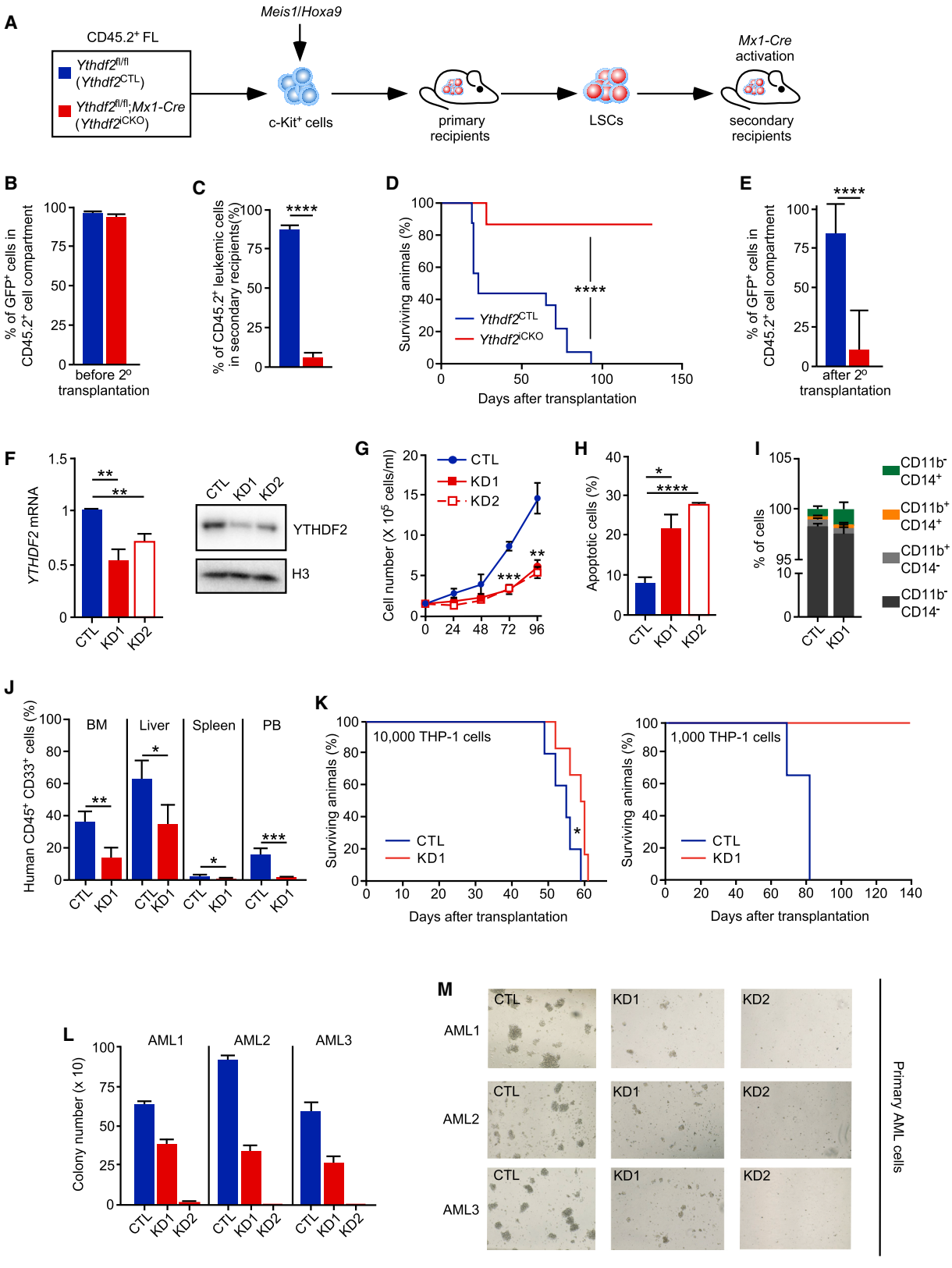

(legend on next page)

Ythdf2 Is Critical for AML Propagation

We next asked whether acute deletion of *Ythdf2* from established LSCs using *Mx1-Cre* impacts LSC maintenance and leukemia propagation. We generated experimental *Ythdf2*$^{fl/fl}$*; Mx1-Cre* (*Ythdf2*^{iCKO}) and control *Ythdf2*$^{fl/fl}$ (*Ythdf2*^{CTL}) mice, transduced HSPCs with *Meis1-Hoxa9* retroviruses, and transplanted them into lethally irradiated primary recipients (Figure 2A). Upon leukemia development, c-Kit$^+$ cells (a population enriched for LSCs; Somervaille and Cleary, 2006) were isolated, and given the leakiness of *Mx1-Cre* upon transplantation (Velasco-Hernandez et al., 2016), the population was further sorted for GFP$^+$ cells to enrich for those expressing YTHDF2 (Figure 2B). While *Ythdf2*^{CTL} c-Kit$^+$GFP$^+$ cells showed significant engraftment and caused aggressive AML in secondary recipients (Figures 2C and 2D), *Ythdf2*^{iCKO} c-Kit$^+$GFP$^+$ cells lost YTHDF2 expression (Figure 2E) due to spontaneous *Mx1-Cre* activation (even without the administration of polyinosinic-polycytidylic acid [pIpC]) and failed to efficiently engraft and propagate the disease (Figures 2C and 2D). Therefore, YTHDF2 is critical for LSC maintenance.

Targeting YTHDF2 Disables Human AML Cells

To investigate the requirement for YTHDF2 in human leukemic cells, we knocked down the expression of *YTHDF2* in human AML THP-1 cells harboring MLL-AF9 translocation using two independent short hairpins targeting *YTHDF2*. *YTHDF2* knockdown (Figure 2F) inhibited their proliferative capacity (Figure 2G) and increased their apoptosis (Figure 2H) but had no impact on their myeloid differentiation (Figure 2I). This finding was corroborated in NOMO-1 AML cells harboring MLL-AF9 translocation (Figures S1B and S1C). THP-1 cells with *YTHDF2* knockdown had compromised capacity to engraft AML (Figure 2J) and displayed impaired ability to cause fatal AML (Figure 2K). Finally, we performed knockdown experiments in independent human primary AML samples and found that *YTHDF2* depletion significantly decreased the clonogenic potential of AML cells in colony-forming cell (CFC) assays (Figures 2L and 2M). Thus, YTHDF2 is necessary for human AML cell survival and leukemic cell engraftment.

Ythdf2 Deletion Does Not Derail Normal Hematopoiesis

We next investigated whether *Ythdf2* deletion has any detrimental effects on HSC functions and multilineage hematopoiesis. To determine the YTHDF2 expression at different levels of the hematopoietic differentiation hierarchy, we employed *Ythdf2*$^{fl/fl}$ mice harboring the GFP-YTHDF2 fusion protein (Ivanova et al., 2017). All hematopoietic cells in adult BM expressed GFP-YTHDF2 (Figures 3A and S2A). YTHDF2 was highly expressed in Lin$^-$Sca-1$^+$c-Kit$^+$ (LSK) stem and/or progenitor cells, HSCs, multipotent progenitors (MPPs), primitive hematopoietic progenitors (HPC-1 and HPC-2 populations), and myeloid progenitors, and its expression was decreased in differentiated Lin$^+$ cells (Figures 3A and S2A).

Peripheral blood (PB) analyses of *Ythdf2*^{CKO} mice revealed modest decreases in numbers of white blood cells (WBCs), red blood cells (RBCs), B cells, and CD8$^+$ T cells and elevated platelet levels (Figure 3B). Apart from a decrease in CD8$^+$ T cells, *Ythdf2*^{CKO} mice had essentially normal numbers of differentiated cells in their spleens (Figure S2B). We found unaffected numbers of granulocyte/macrophage progenitors (GMPs), increased numbers of pre-megakaryocyte/erythroid progenitors (pre-MegEs) and megakaryocyte progenitors (MkPs) and an imbalance between pre-colony forming unit-erythroid (pre-CFU-E) and colony forming unit-erythroid (CFU-E) (Figure S2C). CFC assays showed normal differentiation potential of *Ythdf2*^{CKO} BM cells (Figure 3C). Thus, YTHDF2 is not critical for steady-state hematopoiesis.

Ythdf2 Loss Results in HSC Expansion

We next investigated the impact of *Ythdf2* deletion on stem and progenitor cells. Adult *Ythdf2*^{CKO} mice displayed expansion of LSK cells, HSCs, and HPC-1 and HPC-2 progenitor cells compared to *Ythdf2*^{CTL} mice (Figures 3D and 3E). We also inducibly ablated *Ythdf2* using *Mx1-Cre*, which upon pIpC injection acutely deletes *Ythdf2* in *Ythdf2*^{iCKO} adult mice (Figure 3F). Acute *Ythdf2* deletion (Figure 3G) had no impact on mouse survival (data not shown) or multilineage hematopoiesis (Figures 3H and 3I; Table S1) and resulted in increased numbers of LSK cells, but not myeloid progenitor cells (Figure 3J). Thus,

Figure 2. Loss of YTHDF2 from Established LSCs and Human AML Cells Compromises Their Ability to Propagate AML

(A) *Ythdf2*$^{fl/fl}$ (*Ythdf2*^{CTL}) and *Ythdf2*$^{fl/fl}$*;Mx1-Cre* (*Ythdf2*^{iCKO}) FL c-Kit$^+$ cells were co-transduced with *Meis1* and *Hoxa9* retroviruses, serially replated, and transplanted into primary recipients. GFP$^+$c-Kit$^+$CD45.2$^+$ cells sorted from leukemic primary recipients were re-transplanted into secondary recipients (n = 14–16).

(B) Percentage of GFP-expressing cells as a measure of YTHDF2 expression in *Ythdf2*^{CTL} and *Ythdf2*^{iCKO} leukemic cells prior to secondary transplantation.

(C) Percentage of CD45.2$^+$ leukemic cells in the PB of the secondary recipient mice 3 weeks after transplantation (n = 14–16 recipients).

(D) Survival curve of mice transplanted with *Ythdf2*^{CTL} and *Ythdf2*^{iCKO} leukemic cells (n = 14–16 mice).

(E) Percentage of GFP-expressing cells in PB CD45.2$^+$ cell compartment of secondary recipient mice.

(F) Left: relative levels of *YTHDF2* mRNA (normalized to *HPRT1*) in human AML THP-1 cells transduced with lentiviruses expressing scrambled short hairpin RNA (shRNA) (CTL) and two independent shRNAs targeting *YTHDF2* (KD1 and KD2); n = 3. Right: western blot of YTHDF2 in THP-1 cells shown on the left. α-Histone 3 (H3) was used as a loading control.

(G) Proliferation assays with THP-1 cells with CTL, KD1, and KD2 shRNAs.

(H) Percentage of Annexin V$^+$DAPI$^-$ cells.

(I) Percentage of CD11b$^-$CD14$^-$, CD11b$^+$CD14$^-$, CD11b$^+$CD14$^+$, and CD11b$^-$CD14$^+$ cells in cultures shown in (G) and (H).

(J) NSG mice were injected with THP-1 cells transduced with CTL (n = 4) or KD (n = 4) lentiviruses and analyzed 1 month later. Percentage of human CD45$^+$CD33$^+$ cells in the BM, liver, spleen, and PB of the recipient mice is shown.

(K) Survival curve of mice transplanted with 10,000 (n = 6) and 1,000 (n = 3) THP-1 cells.

(L) Three independent human primary AML samples (AML1–AML3; detailed in STAR Methods) were transduced with CTL, KD1, and KD2 lentiviruses. The graph shows AML-CFC frequencies after 7 days of culture (n = 3 technical replicates per sample).

(M) Representative colony images from (L).

Data represent mean ± SEM in (A)–(K) or mean ± SD in (L)–(M); *p < 0.05; **p < 0.01; ***p < 0.001; ****p < 0.0001.

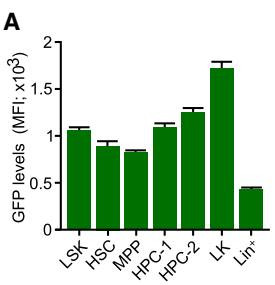

B

	Ythdf2^{CTL}	*Ythdf2*^{CKO}	P value
WBC (/μl)	9767 ± 935	7214 ± 2292	0.0479
RBC (X10^4/μl)	1178 ± 23.61	1071 ± 22.87	0.0051
Hb (g/dl)	16.91 ± 0.3513	15.97 ± 0.3803	0.1085
PLT (X10^4/μl)	80.78 ± 3.896	100.2 ± 5.841	0.0460
CD4$^+$ T cells (/μl)	1459 ± 176.7	1161 ± 168.2	0.1135
CD8$^+$ T cells (/μl)	1102 ± 178.6	530.5 ± 92.22	0.0206
B cells (/μl)	5226 ± 575.6	3828 ± 182.3	0.0206
Granulocytes (/μl)	2112 ± 458.5	1510 ± 361.7	0.3655
Monocytes (/μl)	390.8 ± 41.93	442.3± 26.04	0.2320

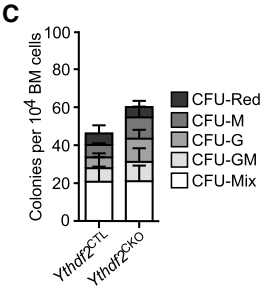

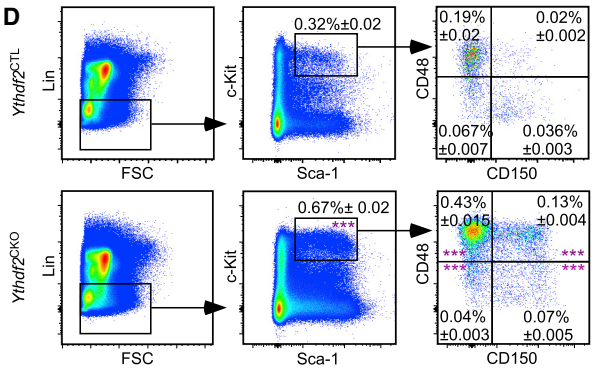

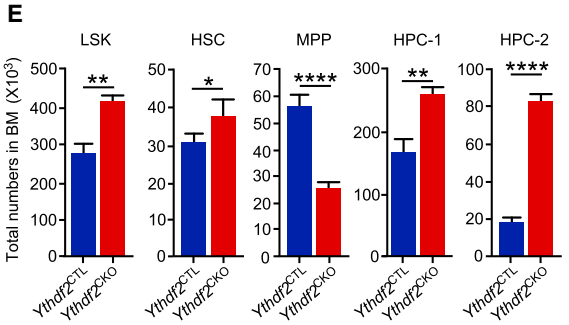

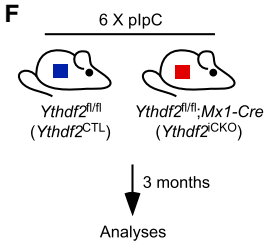

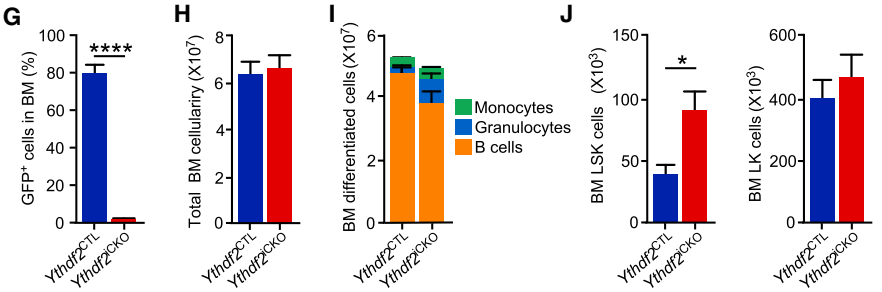

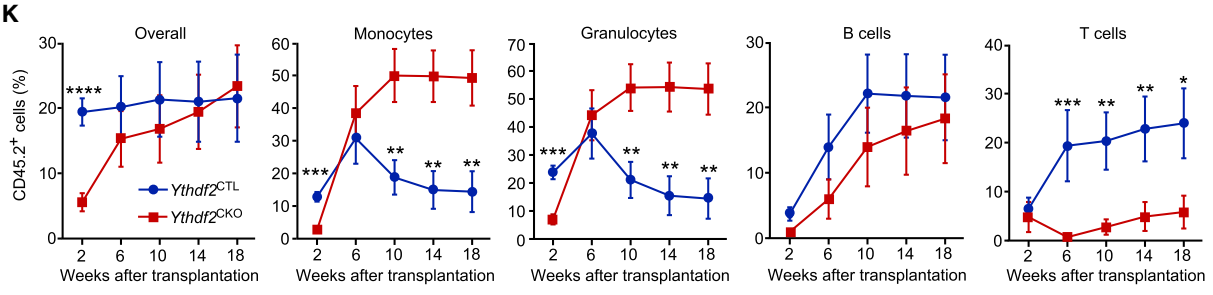

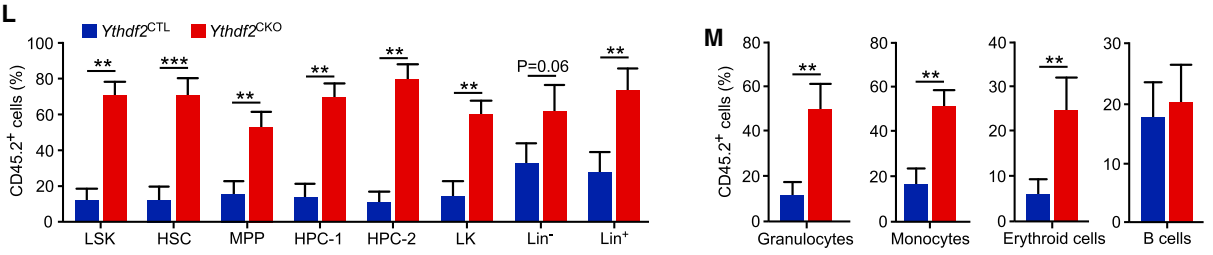

(legend on next page)

hematopoiesis-specific *Ythdf2* ablation during development or acute deletion in adult mice leads to an expansion of the primitive cell compartment at the top of the hematopoietic hierarchy and does not derail normal hematopoiesis.

To reveal the repopulation capacity of *Ythdf2*-deficient HSCs, we competitively transplanted HSCs from *Ythdf2*^{CKO} and *Ythdf2*^{CTL} mice into lethally irradiated recipients. HSCs of both genotypes gave equal overall long-term reconstitution (Figure 3K). However, while *Ythdf2*^{CKO} HSCs had enhanced myeloid lineage reconstitution capacity, they had normal B cell and compromised T cell reconstitution potentials (Figure 3K). Strikingly, *Ythdf2*^{CKO} HSCs displayed significantly increased capacity to contribute to the BM HSC and progenitor cell compartments and differentiated cell compartments (Figures 3L and 3M). The analyses of donor-derived compartment of the recipients revealed increased frequencies of *Ythdf2*^{CKO} LSK, HPC-1, and HPC-2 cells (Figure S2D). The myeloid bias of *Ythdf2*-deficient HSCs and its connection to a shift in balance among the HSCs, MPP, and HPC populations upon *Ythdf2* deletion merit future investigation. Therefore, targeting *Ythdf2* promotes stem or primitive progenitor cell expansion and enhances their reconstitution and myeloid differentiation potentials.

YTHDF2 Decreases m^{6}A RNA Stability in AML

We next sought to understand the mechanism by which YTHDF2 loss impedes LSC function. YTHDF2 is known to promote transcript decay through deadenylation (Du et al., 2016; Wang et al., 2014a). Indeed, the loss of YTHDF2 resulted in deregulated gene expression with 754 upregulated and 528 downregulated genes; $p < 0.05$) in *Ythdf2*^{CKO} compared to *Ythdf2*^{CTL} preleukemic cells (Figure 4A). Gene Ontology analysis of deregulated genes in preleukemic cells revealed generic metabolic processes in the upregulated genes and immune response processes in the downregulated genes (Figure S3A). To understand which of the deregulated transcripts could be direct targets of YTHDF2, we determined transcriptome-wide mRNA m^{6}A in *Ythdf2*^{CTL} and *Ythdf2*^{CKO} preleukemic cells. This revealed the expected m^{6}A consensus motif as well as distribution of m^{6}A within the transcriptome and enrichment around the stop codon within transcripts in both genotypes (Figures S3B–S3D). Furthermore, *Ythdf2* deficiency did not alter any of these parameters (Figures S3B–S3D). YTHDF2 loss is expected to result in the upregulation of direct target transcripts; indeed, we observed an enrichment for m^{6}A occupancy in the significantly upregulated genes ($p < 0.05$; 754 genes) in *Ythdf2*^{CKO} preleukemic cells compared to the corresponding unchanged or downregulated gene sets (Figure 4B). Reciprocally, we analyzed the transcriptome based on RNA m^{6}A modification and found that transcripts that contain m^{6}A show increased expression in *Ythdf2*^{CKO} preleukemic cells (Figures 4C and 4D). To understand if these observations are extended to the AML *in vivo*, we isolated LSCs from mice with AML derived from *Ythdf2*^{CTL} and *Ythdf2*^{CKO} preleukemic cells and performed gene expression analysis (Figure S3E). The relationship between m^{6}A occupancy and increased transcript dosage was also observed in *Ythdf2*^{CKO} LSCs (Figures S3F–S3H). The upregulation of m^{6}A-containing transcripts in the absence of YTHDF2 may arise from an increase in their half-life. We therefore measured mRNA half-life transcriptome-wide in preleukemic cells using thiol(SH)-linked alkylation for the metabolic sequencing of RNA (SLAM-seq; Herzog et al., 2017), which revealed an overall modest increase in mRNA half-life in *Ythdf2*^{CKO} cells (Figure 4E). Interestingly, m^{6}A-containing transcripts displayed overall shorter half-lives than non-m^{6}A transcripts in *Ythdf2*^{CTL} cells (Figure 4F). YTHDF2 loss extended the half-life of m^{6}A-containing transcripts (Figures 4F and 4G). We next employed ribosome profiling (RIBO-seq; Reid et al., 2015) to measure translational efficiency that did not grossly alter between the respective genotypes (Figure 4H). YTHDF2 deficiency did not alter the translational efficiency of either m^{6}A or non-m^{6}A-containing transcripts (Figure 4I). These data indicate that m^{6}A-directed YTHDF2-mediated mRNA decay contributes to the regulation of the leukemic transcriptome.

Next, we sought to determine if the m^{6}A-modified transcripts deregulated upon *Ythdf2* deletion in mouse AML are relevant to human AML. We found that transcripts significantly upregulated in the *Ythdf2*^{CKO} preleukemic cells are preferentially methylated in human AML cell lines (Figure 4J). To understand the molecular pathways underpinned by upregulated transcripts methylated both in mouse and human, we performed ConcensusPathDB

Figure 3. *Ythdf2* Deletion Results in HSC and Progenitor Cell Expansion and Enhanced HSC Reconstitution Potential

(A) GFP expression in the BM cell populations from 8- to 12-week-old *Ythdf2*$^{fl/fl}$ (*Ythdf2*^{CTL}) mice. YTHDF2 is uniformly expressed in BM Lin$^-$Sca-1$^+$c-Kit$^+$ (LSK) cells, LSKCD48$^-$CD150$^+$ HSCs, LSKCD48$^-$CD150$^-$ multipotent progenitors (MPPs), primitive hematopoietic progenitor cells (i.e., LSKCD48$^+$CD150$^-$ HPC-1 and LSKCD48$^+$CD150$^+$ HPC-2 populations), and Lin$^-$Sca-1$^-$c-Kit$^+$ (LK) myeloid progenitors, and its expression is decreased in differentiated Lin$^+$ cells. Data represent mean fluorescence intensity (MFI) ± SEM (n = 4).

(B) PB counts of *Ythdf2*^{CTL} and *Ythdf2*^{CKO} in 8- to 10-wk-old mice (n = 8–9).

(C) CFU assays performed with BM cells from 8- to 10-wk-old mice. CFU-Red, CFU-erythroid and/or megakaryocyte; CFU-G, CFU-granulocyte; CFU-M, CFU-monocyte/macrophage; CFU-GM, CFU–granulocyte and monocyte/macrophage; CFU-Mix, at least three of the following: granulocyte, erythroid, monocyte/macrophage, and megakaryocyte (n = 4).

(D) FACS profiles showing frequencies (± SEM) of BM LSK, HSC, MPP, HPC-1, and HPC-2 cell populations from *Ythdf2*^{CTL} and *Ythdf2*^{CKO} mice (n = 6–7 mice).

(E) Total number of BM cell populations presented in (D).

(F) *Ythdf2*$^{fl/fl}$;*Mx1-Cre* (*Ythdf2*^{iCKO}) and control *Ythdf2*$^{fl/fl}$ (*Ythdf2*^{CTL}) mice were injected with pIpC and analyzed 3 months after the last injection.

(G) Graph showing the percentage of GFP-positive cells in BM of pIpC-treated *Ythdf2*^{iCKO} and *Ythdf2*^{CTL} mice (n = 10–12).

(H) Total BM cellularity of pIpC-treated *Ythdf2*^{iCKO} and *Ythdf2*^{CTL} mice.

(I) Total cell numbers of BM monocytes, granulocytes, and B cells.

(J) Total cell numbers of BM LSK and LK cell populations.

(K) HSCs were transplanted into lethally irradiated recipient mice (n = 6–9) together with competitor BM cells. Graph shows the percentage of CD45.2$^+$ cells overall in the PB and in the monocyte, granulocyte, B cell, and T cell compartments of the PB of primary recipients.

(L and M) Percentage of CD45.2$^+$ cells in the Lin$^+$, Lin$^-$, LK, LSK, and HSC (L) and differentiated (M) cell compartments in the BM of recipient mice.

Data represent mean ± SEM; *$p < 0.05$; **$p < 0.01$; ***$p < 0.001$; ****$p < 0.0001$.

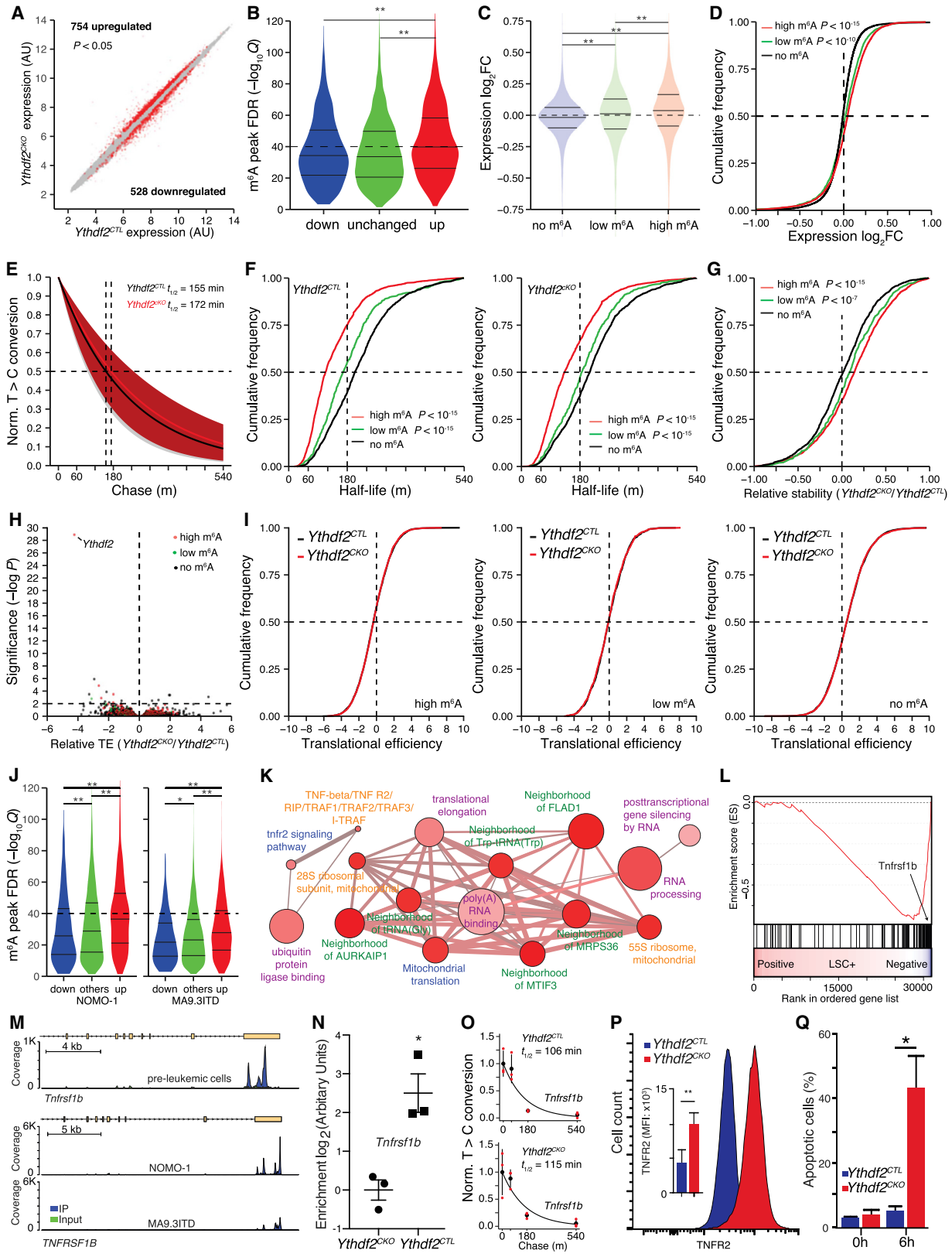

(legend on next page)

(CPDB) network analysis and found enrichment for RNA processing, mitochondrial function, ubiquitination as well as tumor necrosis factor (TNF) signaling (Figures 4K and S3I). To reveal why the loss of YTHDF2 is correlated with a weak leukemogenic potential, we interrogated gene sets from human AML samples associated with different leukemogenic potential in *vivo* (Ng et al., 2016). The upregulated transcripts in *Ythdf2*^{CKO} preleukemic cells that contain m^{6}A in both mouse and human AML cells were divided into groups whose expression positively or negatively correlates with YTHDF2 expression in 1,732 human AML samples (Figure S3I). We found that transcripts that negatively correlate with YTHDF2 expression are highly associated with the loss of leukemogenic potential (Figure 4L). In this way, when an AML sample expresses low amounts of YTHDF2, transcripts associated with the loss of leukemogenic potential have greater expression. In contrast, transcripts whose expression correlates with that of YTHDF2 are depleted from transcripts associated with weak LSC activity (Figure S3J). Thus, YTHDF2 negatively regulates transcripts whose expression limits LSC activity.

Ythdf2 Deletion Sensitizes AML Cells to TNF

Inspecting the genes that negatively correlate with YTHDF2 expression in human AML, contain m^{6}A in both mouse and human AML, are upregulated in *Ythdf2*^{CKO} LSCs, and are associated with weak LSC function, we found TNF receptor 2 (TNFR2) encoded by *Tnfrsf1b* gene (Figure 4L). We focused on TNFR2, as TNF signaling was also identified as a node in the CPDB network analysis (Figure 4K) and TNFR2, together with TNFR1, restricts the accumulation of leukemic cells (Höckendorf et al., 2016). *TNFRSF1B* expression is significantly decreased in AML samples compared to non-leukemic controls (Figure S3K), and its expression negatively correlates with LSC activity (Figure S3L). Notably, *TNFRSF1B* is highly methylated in mouse preleukemic cells and human AML cells (Figure 4M). RNA immunoprecipitation (RIP)-qPCR revealed co-precipitation of the *Tnfrsf1b* transcript with YTHDF2 (Figure 4N). Concurrent with the increased half-life of *Tnfrsf1b* transcript (Figure 4O), the surface expression of TNFR2 is upregulated on *Ythdf2*^{CKO} preleukemic cells (Figure 4P). We therefore tested if TNF stimulation had differential impact on *Ythdf2*^{CTL} and *Ythdf2*^{CKO} preleukemic cells. YTHDF2 loss rendered cells more sensitive to TNF-induced apoptosis (Figure 4Q). This highlights at least one molecular mechanism by which YTHDF2 loss negatively impacts AML.

DISCUSSION

Through the analysis of mRNA m^{6}A methyltransferases and demethylase, a key role for mRNA m^{6}A has been shown in AML pathogenesis (Barbieri et al., 2017; Li et al., 2017; Vu et al., 2017; Weng et al., 2018). The modification of mRNA with m^{6}A can have multiple outcomes on the respective transcript (Zhao et al., 2017), but here we demonstrate that the YTHDF2-mediated

Figure 4. YTHDF2 Targets m^{6}A-Methylated Transcripts for Degradation

(A) Transcript expression scatterplot from *Ythdf2*^{CTL} and *Ythdf2*^{CKO} preleukemic cells (n = 5). Significantly upregulated or downregulated transcripts are highlighted in red ($p < 0.05$).

(B) m^{6}A peak false discovery rate (FDR) ($-\log_{10}$Q) in *Ythdf2*^{CTL} preleukemic cells for transcripts grouped according to expression changes between *Ythdf2*^{CTL} and *Ythdf2*^{CKO} preleukemic cells is shown (down, genes significantly downregulated in *Ythdf2*^{CKO} [$p < 0.05$]; unchanged, genes not significantly changing in *Ythdf2*^{CKO}; up, genes significantly upregulated in *Ythdf2*^{CKO} [$p < 0.05$]). The upper and lower quartiles and the median are shown for each group.

(C) Violin plots showing expression change between *Ythdf2*^{CTL} and *Ythdf2*^{CKO} preleukemic cells for not-methylated (no m^{6}A), methylated (m^{6}A, $-\log_{10}Q \leq 25$), and highly methylated (m^{6}A high, $-\log_{10}Q > 25$) transcripts. The upper and lower quartiles and the median are indicated for each group.

(D) Cumulative distributions of transcript expression change in *Ythdf2*^{CTL} and *Ythdf2*^{CKO} preleukemic cells for not-methylated, methylated, and highly methylated transcripts as in (C).

(E) Mode decay curves for *Ythdf2*^{CTL} (black) and *Ythdf2*^{CKO} (red) preleukemic cell transcriptomes are shown. The shaded areas indicate the first and third quantile decay curves range for each genotype. Transcript half-life modes for each genotype are indicated with horizontal dotted lines and are also shown at the panel top.

(F) Cumulative distributions of transcript half-life in *Ythdf2*^{CTL} (left) and *Ythdf2*^{CKO} (right) preleukemic cells are shown for not methylated, methylated and highly methylated transcripts as in (C). The half-life change significance between methylated and not-methylated transcripts is indicated.

(G) Cumulative distributions of relative stability change between *Ythdf2*^{CTL} and *Ythdf2*^{CKO} preleukemic cells are shown for not-methylated, methylated, and highly methylated transcripts as in (C). The relative stability change significances between the methylated and not methylated transcripts are indicated.

(H) Volcano plot of translational efficiency change between *Ythdf2*^{CTL} and *Ythdf2*^{CKO} preleukemic cells. Not-methylated, methylated, and highly methylated transcripts defined as in (C) are shown in black, green, and red, respectively.

(I) Cumulative distributions of translational efficiency of not-methylated (right), methylated (middle), and highly methylated transcripts (left) defined as in (C) are shown for *Ythdf2*^{CTL} (black) and *Ythdf2*^{CKO} (red) preleukemic cells.

(J) Violin plots of m^{6}A peak FDR ($-\log_{10}Q$) in MA9.3ITD and NOMO-1 cells for transcripts grouped according to expression changes between *Ythdf2*^{CTL} and *Ythdf2*^{CKO} preleukemic cells as in (B) are shown. The upper and lower quartiles and the median are indicated for each group.

(K) CPDB analysis of genes significantly upregulated in *Ythdf2*^{CKO} preleukemic cells ($p < 0.05$) with high m^{6}A levels ($-\log_{10}Q > 25$) in mouse preleukemic cells and also methylated in human AML cell lines.

(L) GSEA using LSC signature gene set for genes defined in (K) and that negatively correlate with *YTHDF2* expression in human AML samples.

(M) m^{6}A immunoprecipitation (IP) read coverage (blue) from *Ythdf2*^{CTL} preleukemic cells along the *Tnfrs1b* genomic locus (top) and m^{6}A IP read coverage from NOMO-1, and MA9.3ITD cells along the *TNFRSF1B* genomic locus (bottom) are shown. Input coverage is shown in green.

(N) *Tnfrsf1b* enrichment in YTHDF2 immunoprecipitates from *Ythdf2*^{CTL} preleukemic cells is shown. *Tnfrsf1b* background levels were determined using *Ythdf2*^{CKO} preleukemic cells (n = 3).

(O) Decay curves for *Trnfrs1b* in *Ythdf2*^{CTL} (top) and *Ythdf2*^{CKO} (bottom) preleukemic cells transcriptomes are shown. The center value and the error bars at each time point indicate the conversion rate mean and SD, respectively. The conversion rates for each biological replicate are indicated with dots. The *Trnfrs1b* half-life is also shown.

(P) FACS plots showing the expression of TNFR2 on the cell surface of *Ythdf2*^{CTL} and *Ythdf2*^{CKO} preleukemic cells. The inner graph displays the quantification of TNFR2 expression (n = 4).

(Q) Percentage of Annexin V$^+$DAPI$^-$ preleukemic cells treated with TNF-α at 0-h and 6-h time points (n = 3).

Data in (N), (P), and (Q) represent mean ± SEM. In (B), (C), (J), (N), (P), and (Q) *$p < 0.05$; **$p < 0.01$.

component of the pathway is also critical for cancer stem cells in AML. We find that inhibition of YTHDF2 specifically compromises LSC development and propagation. Given the more severe impact of *Ythdf2* deletion or knockdown on established AML compared to disease development, AML propagation may be even more dependent on YTHDF2 than disease initiation. Furthermore, consistent with recent findings in mouse and human HSCs (Li et al., 2018; Wang et al., 2018), we demonstrate that targeting *Ythdf2* expands HSCs and enhances their myeloid reconstitution. These are unique properties of YTHDF2, which, coupled with the fact that the loss of YTHDF2 is permissive in adult mice, underscores the therapeutic potential of YTHDF2 inhibition as a strategy for AML treatment. Such an intervention would have the dual benefits of eradicating malignant LSCs while bestowing a competitive advantage to normal HSCs. Given that isolation of HSCs in sufficient quantities is a limiting factor for the usage of HSC transplantation for a variety of diseases, inhibition of YTHDF2 could be employed to expand HSCs *in vitro* or *in vivo* to circumvent this challenge. In summary, we revealed the m^{6}A reader YTHDF2 as a critical mediator of LSCs whose inhibition selectively compromises AML implying its future applications in treatment of this hematological malignancy.

STAR★METHODS

Detailed methods are provided in the online version of this paper and include the following:

- KEY RESOURCES TABLE
- CONTACT FOR REAGENT AND RESOURCE SHARING
- EXPERIMENTAL MODEL AND SUBJECT DETAILS
  - Mice
  - Human tissue & ethical approvals
- METHOD DETAILS
  - Flow cytometry
  - Colony forming cells (CFC) assays
  - Leukemic transformation
  - Syngeneic transplantation assays
  - Xenotransplantation experiments
  - pIpC administration
  - shRNA-mediated YTHDF2 knockdown
  - Cell proliferation, cell death and cell differentiation analyses
  - Primary human AML patient derived samples
  - Western blotting
  - Affymetrix
  - Analyses of YTHDF2 expression in human AML samples
  - m^{6}A meRIP-Seq
  - SLAM-seq
  - RIBO-seq
- DATA AND SOFTWARE AVAILABILITY
  - Accession
- QUANTIFICATION AND STATISTICAL ANALYSIS

SUPPLEMENTAL INFORMATION

Supplemental Information can be found online at https://doi.org/10.1016/j.stem.2019.03.021.

ACKNOWLEDGMENTS

K.R.K. is a Cancer Research UK (CRUK) Senior Cancer Research Fellow and a CRUK Programme Grant holder. This work is funded by CRUK (awards C29967/A14633 and C29967/A26787 to K.R.K.) and Wellcome (award 106144 to D.O.). K.R.K.'s laboratory is also supported by grants from The Barts Charity, Wellcome, Bloodwise, Medical Research Council, and the Kay Kendall Leukaemia Fund. D.O. is a member of the Wellcome Centre for Cell Biology supported by Wellcome core funding (award 092076). G.J.S. and T.C.P.S. are supported by CRUK (award C5759/A20971). Part of this work was carried out in the framework of the European Cost Action EPITRAN CA16120. We thank Vladimir Benes and Jelena Pistolic (Genomics Core facility, European Molecular Biology Laboratory, Heidelberg) for performing the gene expression profiling. Brian Huntly and Eric So kindly provided *MOZ-TIF2* and *PML-RARA* plasmids, respectively.

AUTHOR CONTRIBUTIONS

K.R.K. and D.O. designed experiments and wrote the paper. J.P. and J. Campos performed all *in vivo* experiments and FACS analyses and helped with writing the manuscript. M.M. performed computational analyses of m^{6}A-seq, SLAM-seq RIBO-seq, and gene expression profiling. A.N., F.M., and L.N.v.d.L. performed bioinformatic analyses of publicly available AML datasets. M.M., A. Shmakova, A. Sarapuu, C. Mapperley, I.I., H.L., D.A.W., C.S., M.V., A.V.G., A.V., C. Much, L.A., D.V., A.T., and A.A. helped with experiments and data analyses. J. Choe and R.I.G. performed m^{6}A-seq. G.J.S. and T.C.P.S. performed experiments on primary AML cells. J.P., M.M., and J. Campos contributed equally to this work. K.R.K. and D.O. contributed equally to this work.

DECLARATION OF INTERESTS

K.R.K. and D.O. are inventors on patent number GB 1805287.8.

Received: May 4, 2018
Revised: February 20, 2019
Accepted: March 22, 2019
Published: April 25, 2019

REFERENCES

Bachas, C., Schuurhuis, G.J., Zwaan, C.M., van den Heuvel-Eibrink, M.M., den Boer, M.L., de Bont, E.S., Kwidama, Z.J., Reinhardt, D., Creutzig, U., de Haas, V., et al. (2015). Gene expression profiles associated with pediatric relapsed AML. PLoS ONE *10*, e0121730.

Barbieri, I., Tzelepis, K., Pandolfini, L., Shi, J., Millán-Zambrano, G., Robson, S.C., Aspris, D., Migliori, V., Bannister, A.J., Han, N., et al. (2017). Promoter-bound METTL3 maintains myeloid leukaemia by m^{6}A-dependent translation control. Nature *552*, 126–131.

Benjamini, Y., and Hochberg, Y. (1995). Controlling the false discovery rate: a practical and powerful approach to multiple testing. J. R. Stat. Soc. Series B Stat. Methodol. *57*, 289–300.

Bokar, J.A., Shambaugh, M.E., Polayes, D., Matera, A.G., and Rottman, F.M. (1997). Purification and cDNA cloning of the AdoMet-binding subunit of the human mRNA (N6-adenosine)-methyltransferase. RNA *3*, 1233–1247.

Bray, N.L., Pimentel, H., Melsted, P., and Pachter, L. (2016). Near-optimal probabilistic RNA-seq quantification. Nat. Biotechnol. *34*, 525–527.

de Boer, J., Williams, A., Skavdis, G., Harker, N., Coles, M., Tolaini, M., Norton, T., Williams, K., Roderick, K., Potocnik, A.J., and Kioussis, D. (2003). Transgenic mice with hematopoietic and lymphoid specific expression of Cre. Eur. J. Immunol. *33*, 314–325.

Desrosiers, R., Friderici, K., and Rottman, F. (1974). Identification of methylated nucleosides in messenger RNA from Novikoff hepatoma cells. Proc. Natl. Acad. Sci. USA *71*, 3971–3975.

Döhner, H., Weisdorf, D.J., and Bloomfield, C.D. (2015). Acute myeloid leukemia. N. Engl. J. Med. *373*, 1136–1152.

Drabkin, H.A., Parsy, C., Ferguson, K., Guilhot, F., Lacotte, L., Roy, L., Zeng, C., Baron, A., Hunger, S.P., Varella-Garcia, M., et al. (2002). Quantitative HOX expression in chromosomally defined subsets of acute myelogenous leukemia. Leukemia *16*, 186–195.

Du, H., Zhao, Y., He, J., Zhang, Y., Xi, H., Liu, M., Ma, J., and Wu, L. (2016). YTHDF2 destabilizes m(6)A-containing RNA through direct recruitment of the CCR4-NOT deadenylase complex. Nat. Commun. *7*, 12626.

Eppert, K., Takenaka, K., Lechman, E.R., Waldron, L., Nilsson, B., van Galen, P., Metzeler, K.H., Poeppl, A., Ling, V., Beyene, J., et al. (2011). Stem cell gene expression programs influence clinical outcome in human leukemia. Nat. Med. *17*, 1086–1093.

Esposito, M.T., Zhao, L., Fung, T.K., Rane, J.K., Wilson, A., Martin, N., Gil, J., Leung, A.Y., Ashworth, A., and So, C.W. (2015). Synthetic lethal targeting of oncogenic transcription factors in acute leukemia by PARP inhibitors. Nat Med *21*, 1481–1490.

Fu, Y., Dominissini, D., Rechavi, G., and He, C. (2014). Gene expression regulation mediated through reversible m^6A RNA methylation. Nat. Rev. Genet. *15*, 293–306.

Gentleman, R.C., Carey, V.J., Bates, D.M., Bolstad, B., Dettling, M., Dudoit, S., Ellis, B., Gautier, L., Ge, Y., Gentry, J., et al. (2004). Bioconductor: open software development for computational biology and bioinformatics. Genome Biol. *5*, R80.

Guitart, A.V., Subramani, C., Armesilla-Diaz, A., Smith, G., Sepulveda, C., Gezer, D., Vukovic, M., Dunn, K., Pollard, P., Holyoake, T.L., et al. (2013). Hif-2α is not essential for cell-autonomous hematopoietic stem cell maintenance. Blood *122*, 1741–1745.

Guitart, A.V., Panagopoulou, T.I., Villacreces, A., Vukovic, M., Sepulveda, C., Allen, L., Carter, R.N., van de Lagemaat, L.N., Morgan, M., Giles, P., et al. (2017). Fumarate hydratase is a critical metabolic regulator of hematopoietic stem cell functions. J. Exp. Med. *214*, 719–735.

Haferlach, C., Mecucci, C., Schnittger, S., Kohlmann, A., Mancini, M., Cuneo, A., Testoni, N., Rege-Cambrin, G., Santucci, A., Vignetti, M., et al. (2009). AML with mutated NPM1 carrying a normal or aberrant karyotype show overlapping biologic, pathologic, immunophenotypic, and prognostic features. Blood *114*, 3024–3032.

Haferlach, T., Kohlmann, A., Wieczorek, L., Basso, G., Kronnie, G.T., Béné, M.C., De Vos, J., Hernández, J.M., Hofmann, W.K., Mills, K.I., et al. (2010). Clinical utility of microarray-based gene expression profiling in the diagnosis and subclassification of leukemia: report from the International Microarray Innovations in Leukemia Study Group. J. Clin. Oncol. *28*, 2529–2537.

Hahne, F., and Ivanek, R. (2016). Visualizing genomic data using Gviz and Bioconductor. Methods Mol. Biol. *1418*, 335–351.

Herzog, V.A., Reichholf, B., Neumann, T., Rescheneder, P., Bhat, P., Burkard, T.R., Wlotzka, W., von Haeseler, A., Zuber, J., and Ameres, S.L. (2017). Thiol-linked alkylation of RNA to assess expression dynamics. Nat. Methods *14*, 1198–1204.

Höckendorf, U., Yabal, M., Herold, T., Munkhbaatar, E., Rott, S., Jilg, S., Kauschinger, J., Magnani, G., Reisinger, F., Heuser, M., et al. (2016). RIPK3 restricts myeloid leukemogenesis by promoting cell death and differentiation of leukemia initiating cells. Cancer Cell *30*, 75–91.

Huntly, B.J., Shigematsu, H., Deguchi, K., Lee, B.H., Mizuno, S., Duclos, N., Rowan, R., Amaral, S., Curley, D., Williams, I.R., et al. (2004). MOZ-TIF2, but not BCR-ABL, confers properties of leukemic stem cells to committed murine hematopoietic progenitors. Cancer Cell *6*, 587–596.

Ivanova, I., Much, C., Di Giacomo, M., Azzi, C., Morgan, M., Moreira, P.N., Monahan, J., Carrieri, C., Enright, A.J., and O'Carroll, D. (2017). The RNA m6A reader YTHDF2 is essential for the post-transcriptional regulation of the maternal transcriptome and oocyte competence. Mol. Cell *67*, 1059–1067.e1054.

Jia, G., Fu, Y., Zhao, X., Dai, Q., Zheng, G., Yang, Y., Yi, C., Lindahl, T., Pan, T., Yang, Y.G., and He, C. (2011). N6-methyladenosine in nuclear RNA is a major substrate of the obesity-associated FTO. Nat. Chem. Biol. *7*, 885–887.

Kamburov, A., Stelzl, U., Lehrach, H., and Herwig, R. (2013). The ConsensusPathDB interaction database: 2013 update. Nucleic Acids Res. *41*, D793–D800.

Kauffmann, A., Gentleman, R., and Huber, W. (2009). arrayQualityMetrics—a bioconductor package for quality assessment of microarray data. Bioinformatics *25*, 415–416.

Kim, D., Langmead, B., and Salzberg, S.L. (2015). HISAT: a fast spliced aligner with low memory requirements. Nat. Methods *12*, 357–360.

Klein, H.U., Ruckert, C., Kohlmann, A., Bullinger, L., Thiede, C., Haferlach, T., and Dugas, M. (2009). Quantitative comparison of microarray experiments with published leukemia related gene expression signatures. BMC Bioinformatics *10*, 422.

Kranc, K.R., Schepers, H., Rodrigues, N.P., Bamforth, S., Villadsen, E., Ferry, H., Bouriez-Jones, T., Sigvardsson, M., Bhattacharya, S., Jacobsen, S.E., and Enver, T. (2009). Cited2 is an essential regulator of adult hematopoietic stem cells. Cell Stem Cell *5*, 659–665.

Kroon, E., Krosl, J., Thorsteinsdottir, U., Baban, S., Buchberg, A.M., and Sauvageau, G. (1998). Hoxa9 transforms primary bone marrow cells through specific collaboration with Meis1a but not Pbx1b. EMBO J. *17*, 3714–3725.

Kühn, R., Schwenk, F., Aguet, M., and Rajewsky, K. (1995). Inducible gene targeting in mice. Science *269*, 1427–1429.

Lawrence, H.J., Rozenfeld, S., Cruz, C., Matsukuma, K., Kwong, A., Kömüves, L., Buchberg, A.M., and Largman, C. (1999). Frequent co-expression of the HOXA9 and MEIS1 homeobox genes in human myeloid leukemias. Leukemia *13*, 1993–1999.

Li, Z., Weng, H., Su, R., Weng, X., Zuo, Z., Li, C., Huang, H., Nachtergaele, S., Dong, L., Hu, C., et al. (2017). FTO plays an oncogenic role in acute myeloid leukemia as a N^6-methyladenosine RNA demethylase. Cancer Cell *31*, 127–141.

Li, Z., Qian, P., Shao, W., Shi, H., He, X.C., Gogol, M., Yu, Z., Wang, Y., Qi, M., Zhu, Y., et al. (2018). Suppression of m^6A reader Ythdf2 promotes hematopoietic stem cell expansion. Cell Res. *28*, 904–917.

Lin, S., Choe, J., Du, P., Triboulet, R., and Gregory, R.I. (2016). The m(6)A methyltransferase METTL3 promotes translation in human cancer cells. Mol. Cell *62*, 335–345.

Liu, J., Yue, Y., Han, D., Wang, X., Fu, Y., Zhang, L., Jia, G., Yu, M., Lu, Z., Deng, X., et al. (2014). A METTL3-METTL14 complex mediates mammalian nuclear RNA N6-adenosine methylation. Nat. Chem. Biol. *10*, 93–95.

Love, M.I., Huber, W., and Anders, S. (2014). Moderated estimation of fold change and dispersion for RNA-seq data with DESeq2. Genome Biol. *15*, 550.

Månsson, R., Tsapogas, P., Akerlund, M., Lagergren, A., Gisler, R., and Sigvardsson, M. (2004). Pearson correlation analysis of microarray data allows for the identification of genetic targets for early B-cell factor. J. Biol. Chem. *279*, 17905–17913.

McCall, M.N., Murakami, P.N., Lukk, M., Huber, W., and Irizarry, R.A. (2011). Assessing affymetrix GeneChip microarray quality. BMC Bioinformatics *12*, 137.

Metzelder, S.K., Michel, C., von Bonin, M., Rehberger, M., Hessmann, E., Inselmann, S., Solovey, M., Wang, Y., Sohlbach, K., Brendel, C., et al. (2015). NFATc1 as a therapeutic target in FLT3-ITD-positive AML. Leukemia *29*, 1470–1477.

Metzeler, K.H., Hummel, M., Bloomfield, C.D., Spiekermann, K., Braess, J., Sauerland, M.C., Heinecke, A., Radmacher, M., Marcucci, G., Whitman, S.P., et al.; Cancer and Leukemia Group B; German AML Cooperative Group (2008). An 86-probe-set gene-expression signature predicts survival in cytogenetically normal acute myeloid leukemia. Blood *112*, 4193–4201.

Mills, K.I., Kohlmann, A., Williams, P.M., Wieczorek, L., Liu, W.M., Li, R., Wei, W., Bowen, D.T., Loeffler, H., Hernandez, J.M., et al. (2009). Microarray-based classifiers and prognosis models identify subgroups with distinct clinical outcomes and high risk of AML transformation of myelodysplastic syndrome. Blood *114*, 1063–1072.

Mortensen, M., Soilleux, E.J., Djordjevic, G., Tripp, R., Lutteropp, M., Sadighi-Akha, E., Stranks, A.J., Glanville, J., Knight, S., Jacobsen, S.E., et al. (2011). The

autophagy protein Atg7 is essential for hematopoietic stem cell maintenance. J. Exp. Med. *208*, 455–467.

Ng, S.W., Mitchell, A., Kennedy, J.A., Chen, W.C., McLeod, J., Ibrahimova, N., Arruda, A., Popescu, A., Gupta, V., Schimmer, A.D., et al. (2016). A 17-gene stemness score for rapid determination of risk in acute leukaemia. Nature *540*, 433–437.

Orkin, S.H., and Zon, L.I. (2008). Hematopoiesis: an evolving paradigm for stem cell biology. Cell *132*, 631–644.

Perry, R.P., and Kelley, D.E. (1974). Existence of methylated messenger-RNA in mouse L cells. Cell *1*, 37–42.

Pigazzi, M., Masetti, R., Bresolin, S., Beghin, A., Di Meglio, A., Gelain, S., Trentin, L., Baron, E., Giordan, M., Zangrando, A., et al. (2011). MLL partner genes drive distinct gene expression profiles and genomic alterations in pediatric acute myeloid leukemia: an AIEOP study. Leukemia *25*, 560–563.

Ping, X.L., Sun, B.F., Wang, L., Xiao, W., Yang, X., Wang, W.J., Adhikari, S., Shi, Y., Lv, Y., Chen, Y.S., et al. (2014). Mammalian WTAP is a regulatory subunit of the RNA N6-methyladenosine methyltransferase. Cell Res. *24*, 177–189.

Quinlan, A.R., and Hall, I.M. (2010). BEDTools: a flexible suite of utilities for comparing genomic features. Bioinformatics *26*, 841–842.

Ramírez, F., Dündar, F., Diehl, S., Grüning, B.A., and Manke, T. (2014). deepTools: a flexible platform for exploring deep-sequencing data. Nucleic Acids Res. *42*, W187–W191.

Reid, D.W., Shenolikar, S., and Nicchitta, C.V. (2015). Simple and inexpensive ribosome profiling analysis of mRNA translation. Methods *91*, 69–74.

Ritchie, M.E., Phipson, B., Wu, D., Hu, Y., Law, C.W., Shi, W., and Smyth, G.K. (2015). limma powers differential expression analyses for RNA-sequencing and microarray studies. Nucleic Acids Res. *43*, e47.

Sarry, J.E., Murphy, K., Perry, R., Sanchez, P.V., Secreto, A., Keefer, C., Swider, C.R., Strzelecki, A.C., Cavelier, C., Récher, C., et al. (2011). Human acute myelogenous leukemia stem cells are rare and heterogeneous when assayed in NOD/SCID/IL2Rγc-deficient mice. J. Clin. Invest. *121*, 384–395.

Shi, H., Wang, X., Lu, Z., Zhao, B.S., Ma, H., Hsu, P.J., Liu, C., and He, C. (2017). YTHDF3 facilitates translation and decay of N^6-methyladenosine-modified RNA. Cell Res. *27*, 315–328.

Somervaille, T.C., and Cleary, M.L. (2006). Identification and characterization of leukemia stem cells in murine MLL-AF9 acute myeloid leukemia. Cancer Cell *10*, 257–268.

Somerville, T.D., Wiseman, D.H., Spencer, G.J., Huang, X., Lynch, J.T., Leong, H.S., Williams, E.L., Cheesman, E., and Somervaille, T.C. (2015). Frequent derepression of the mesenchymal transcription factor gene FOXC1 in acute myeloid leukemia. Cancer Cell *28*, 329–342.

Su, R., Dong, L., Li, C., Nachtergaele, S., Wunderlich, M., Qing, Y., Deng, X., Wang, Y., Weng, X., Hu, C., et al. (2018). R-2HG exhibits anti-tumor activity by targeting FTO/m(6)A/MYC/CEBPA signaling. Cell *172*, 90–105.e123.

Tanabe, A., Tanikawa, K., Tsunetomi, M., Takai, K., Ikeda, H., Konno, J., Torigoe, T., Maeda, H., Kutomi, G., Okita, K., et al. (2016). RNA helicase YTHDC2 promotes cancer metastasis via the enhancement of the efficiency by which HIF-1α mRNA is translated. Cancer Lett. *376*, 34–42.

Taskesen, E., Bullinger, L., Corbacioglu, A., Sanders, M.A., Erpelinck, C.A., Wouters, B.J., van der Poel-van de Luytgaarde, S.C., Damm, F., Krauter, J., Ganser, A., et al. (2011). Prognostic impact, concurrent genetic mutations, and gene expression features of AML with CEBPA mutations in a cohort of 1182 cytogenetically normal AML patients: further evidence for CEBPA double mutant AML as a distinctive disease entity. Blood *117*, 2469–2475.

Tomasson, M.H., Xiang, Z., Walgren, R., Zhao, Y., Kasai, Y., Miner, T., Ries, R.E., Lubman, O., Fremont, D.H., McLellan, M.D., et al. (2008). Somatic mutations and germline sequence variants in the expressed tyrosine kinase genes of patients with de novo acute myeloid leukemia. Blood *111*, 4797–4808.

Tuck, M.T. (1992). The formation of internal 6-methyladenine residues in eucaryotic messenger RNA. Int. J. Biochem. *24*, 379–386.

Velasco-Hernandez, T., Säwén, P., Bryder, D., and Cammenga, J. (2016). Potential pitfalls of the Mx1-Cre system: implications for experimental modeling of normal and malignant hematopoiesis. Stem Cell Reports *7*, 11–18.

Vu, L.P., Pickering, B.F., Cheng, Y., Zaccara, S., Nguyen, D., Minuesa, G., Chou, T., Chow, A., Saletore, Y., MacKay, M., et al. (2017). The N^6-methyladenosine (m^6A)-forming enzyme METTL3 controls myeloid differentiation of normal hematopoietic and leukemia cells. Nat. Med. *23*, 1369–1376.

Vukovic, M., Guitart, A.V., Sepulveda, C., Villacreces, A., O'Duibhir, E., Panagopoulou, T.I., Ivens, A., Menendez-Gonzalez, J., Iglesias, J.M., Allen, L., et al. (2015). Hif-1α and Hif-2α synergize to suppress AML development but are dispensable for disease maintenance. J. Exp. Med. *212*, 2223–2234.

Vukovic, M., Sepulveda, C., Subramani, C., Guitart, A.V., Mohr, J., Allen, L., Panagopoulou, T.I., Paris, J., Lawson, H., Villacreces, A., et al. (2016). Adult hematopoietic stem cells lacking Hif-1α self-renew normally. Blood *127*, 2841–2846.

Wang, X., Lu, Z., Gomez, A., Hon, G.C., Yue, Y., Han, D., Fu, Y., Parisien, M., Dai, Q., Jia, G., et al. (2014a). N6-methyladenosine-dependent regulation of messenger RNA stability. Nature *505*, 117–120.

Wang, Y., Li, Y., Toth, J.I., Petroski, M.D., Zhang, Z., and Zhao, J.C. (2014b). N6-methyladenosine modification destabilizes developmental regulators in embryonic stem cells. Nat. Cell Biol. *16*, 191–198.

Wang, X., Zhao, B.S., Roundtree, I.A., Lu, Z., Han, D., Ma, H., Weng, X., Chen, K., Shi, H., and He, C. (2015). N(6)-methyladenosine modulates messenger RNA translation efficiency. Cell *161*, 1388–1399.

Wang, H., Zuo, H., Liu, J., Wen, F., Gao, Y., Zhu, X., Liu, B., Xiao, F., Wang, W., Huang, G., et al. (2018). Loss of YTHDF2-mediated m^6A-dependent mRNA clearance facilitates hematopoietic stem cell regeneration. Cell Res. *28*, 1035–1038.

Weng, H., Huang, H., Wu, H., Qin, X., Zhao, B.S., Dong, L., Shi, H., Skibbe, J., Shen, C., Hu, C., et al. (2018). METTL14 inhibits hematopoietic stem/progenitor differentiation and promotes leukemogenesis via mRNA m(6)A modification. Cell Stem Cell *22*, 191–205.e9.

Wilson, C.L., and Miller, C.J. (2005). Simpleaffy: a BioConductor package for Affymetrix Quality Control and data analysis. Bioinformatics *21*, 3683–3685.

Xiao, W., Adhikari, S., Dahal, U., Chen, Y.S., Hao, Y.J., Sun, B.F., Sun, H.Y., Li, A., Ping, X.L., Lai, W.Y., et al. (2016a). Nuclear m(6)A reader YTHDC1 regulates mRNA splicing. Mol. Cell *61*, 507–519.

Xiao, Z., Zou, Q., Liu, Y., and Yang, X. (2016b). Genome-wide assessment of differential translations with ribosome profiling data. Nat. Commun. *7*, 11194.

Xu, C., Wang, X., Liu, K., Roundtree, I.A., Tempel, W., Li, Y., Lu, Z., He, C., and Min, J. (2014). Structural basis for selective binding of m6A RNA by the YTHDC1 YTH domain. Nat. Chem. Biol. *10*, 927–929.

Zhang, Y., Liu, T., Meyer, C.A., Eeckhoute, J., Johnson, D.S., Bernstein, B.E., Nusbaum, C., Myers, R.M., Brown, M., Li, W., and Liu, X.S. (2008). Model-based analysis of ChIP-seq (MACS). Genome Biol. *9*, R137.

Zhang, S., Zhao, B.S., Zhou, A., Lin, K., Zheng, S., Lu, Z., Chen, Y., Sulman, E.P., Xie, K., Bogler, O., et al. (2017). m6A demethylase ALKBH5 maintains tumorigenicity of glioblastoma stem-like cells by sustaining FOXM1 expression and cell proliferation program. Cancer Cell *31*, 591–606.e596.

Zhao, B.S., Roundtree, I.A., and He, C. (2017). Post-transcriptional gene regulation by mRNA modifications. Nat. Rev. Mol. Cell Biol. *18*, 31–42.

Zheng, G., Dahl, J.A., Niu, Y., Fedorcsak, P., Huang, C.M., Li, C.J., Vågbø, C.B., Shi, Y., Wang, W.L., Song, S.H., et al. (2013). ALKBH5 is a mammalian RNA demethylase that impacts RNA metabolism and mouse fertility. Mol. Cell *49*, 18–29.

STAR★METHODS

KEY RESOURCES TABLE

REAGENT or RESOURCE	SOURCE	IDENTIFIER
Antibodies		
Anti-Mouse CD4 (Biotin conjugated, clone H129.19)	BD Biosciences	Cat#553649; RRID: AB_394969
Anti-Mouse CD5 (Biotin conjugated, clone 53-7.3)	BD Biosciences	Cat#553019; RRID: AB_394557
Anti-Mouse CD8a (Biotin conjugated, clone 53-6.7)	BD Biosciences	Cat#553029; RRID: AB_394567
Anti-Mouse CD11b (Biotin conjugated, clone M1/70)	BD Biosciences	Cat#553309; RRID: AB_394773
Anti-Mouse CD45R/B220 (Biotin conjugated, clone RA3-6B2)	BD Biosciences	Cat#553086; RRID: AB_394616
Anti-Mouse Ter119 (Biotin conjugated, clone TER-119)	BD Biosciences	Cat#553672; RRID: AB_394985
Anti-Mouse Gr-1/Ly-6G/C (Biotin conjugated, clone RB6-8C5)	BD Biosciences	Cat#553125; RRID: AB_394641
Anti-Mouse c-Kit/CD117 (APC-Cy7 conjugated, clone 2B8)	Biolegend	Cat#105826; RRID: AB_1626278
Anti-Mouse c-Kit/CD117 (APC conjugated, clone 2B8)	Biolegend	Cat#105812; RRID: AB_313221
Anti-Mouse Sca-1 (PB conjugated, clone E13-161.7)	Biolegend	Cat#122520; RRID: AB_2143237
Anti-Mouse Sca-1 (APC-Cy7 conjugated, clone D7)	Biolegend	Cat#108125; RRID: AB_10639725
Anti-Mouse CD48 (PE conjugated, clone HM48-1)	Biolegend	Cat#103406; RRID: AB_313021
Anti-Mouse CD150 (PE-Cy7 conjugated, clone 12F12.2)	Biolegend	Cat#115914; RRID: AB_439797
Anti-Mouse CD45R/B220 (PerCP conjugated, clone RA3-6B2)	Biolegend	Cat#103236; RRID: AB_893354
Anti-Mouse CD19 (APC-Cy7 conjugated, clone 6D5)	Biolegend	Cat#115530; RRID: AB_830707
Anti-Mouse CD11b (PB conjugated, clone M1/70)	Biolegend	Cat#101224; RRID: AB_755986
Anti-Mouse CD11b (PE conjugated, clone M1/70)	Biolegend	Cat#101208; RRID: AB_312791
Anti-Mouse CD11b (APC conjugated, clone M1/70)	Biolegend	Cat101211; RRID: AB_312794
Anti-Mouse Gr-1/Ly-6G/C (PE-Cy7 conjugated, clone RB6-8C5)	Biolegend	Cat#108416; RRID: AB_313381
Anti-Mouse CD8a (APC conjugated, clone 53-6.7)	Biolegend	Cat#100712; RRID: AB_312751
Anti-Mouse CD8a (PE conjugated, clone 53-6.7)	Biolegend	Cat#100708; RRID: AB_312747
Anti-Mouse CD4 (PE conjugated, clone H129.19)	Biolegend	Cat#130310; RRID: AB_2075573
Anti-Mouse CD45.1 (BV711 conjugated, clone A20)	Biolegend	Cat#110739; RRID: AB_2562605
Anti-Mouse CD45.2 (PB conjugated, clone 104)	Biolegend	Cat#109820; RRID: AB_492872
Anti-Mouse Ter119 (APC conjugated, clone TER-119)	eBiosciences	Cat#17-5921; RRID: AB_469473
Anti-Mouse CD120b/TNFRII (PE conjugated, clone TR75-89)	Biolegend	Cat#113405; RRID: AB_2206942
Anti-human CD45 (PE conjugated, clone 2D1)	Biolegend	Cat#368509; RRID: AB_2566369
Anti-human CD33 (APC conjugated, clone WM53)	Biolegend	Cat#303407; RRID: AB_314351
Anti-human CD11b (APC conjugated, clone ICRF44)	Biolegend	301309; RRID: AB_314161
Anti-human CD14 (PE conjugated, clone 63D3)	Biolegend	367103; RRID: AB_2565887
Annexin-V (PE conjugated)	BD Biosciences	556421
TO-PRO-3	Life Technologies	Cat#T3605
DAPI	Life Technologies	Cat#D1306; RRID: AB_2629482
Streptavidin (PerCP conjugated)	Biolegend	Cat#405213
Fc Block (clone 2.4G2)	BD Biosciences	Cat#553142; RRID: AB_3946587
Western blotting α-YTHDF2	Proteintech	Cat#24744-1-AP; RRID: AB_2687435
Western blotting α-Histone 3 (H3)	abcam	Cat#ab1791; RRID: AB_302613
Bacterial and Virus Strains		
MSCV-Meis1a-puro	Gift from Tim Somerville	Sommerville et al., 2015
MSCV-Hoxa9-neo	Gift from Tim Somerville	Sommerville et al., 2015
MSCV-PML-RARA	Gift from Eric So	Esposito et al., 2015
MSCV-MOZ-TIF2	Gift from Brian Huntly	Huntly et al., 2004
pLKO.1-puro Empty Vector Control Plasmid DNA	Sigma-Aldrich	Cat#SHC001

(*Continued on next page*)

Continued

REAGENT or RESOURCE	SOURCE	IDENTIFIER
Biological Samples		
Primary human AML samples	Manchester Cancer Research Centre Tissue Biobank	N/A
Chemicals, Peptides, and Recombinant Proteins		
Polyinosinic-polycytidylic acid (pIpC)	GE Healthcare	Cat#C27-4732-01
TRIzol	Thermo Fisher Scientific	Cat#15596026
Micrococcal nuclease (MNase)	Roche Applied Science	Cat#10107921001
PNK	New England Biolabs	Cat#M0201S
TNF-α	PeproTech	Cat#315-01A-5
IL-6	Biolegend	Cat#575706
G-CSF	Biolegend	Cat# 578602
TPO	Biolegend	Cat#593306
IL-3	Biolegend	Cat#575506
SCF	Biolegend	Cat#579708
GM-SCF	Biolegend	Cat#576306
SuperSignal West Dura Extended Duration Substrate	Thermo Fisher Scientific	Cat#34075
Critical Commercial Assays		
Ambion WT Expression kit	Ambion	Cat#4491974
Affymetrix, WT Terminal and Control Kits	Affymetrix	Cat#901524
Lexogen Catabolic kit	Lexogen	Cat#062.24
Lexogen QuantSeq 3′ mRNA-Seq Library Prep Kit	Lexogen	Cat#015.24
NEBNext® Multiplex Small RNA Library Prep Set	New England Biolabs	Cat#E7580S
Epicenter Ribo-zero kit	Epicenter	Cat#MRZH116
SENSE Total RNA-Seq Library Prep Kit	Lexogen	Cat#009.08
15% Novex TBE-Urea Gel	Thermo Fisher Scientific	Cat#EC6885BOX
Bolt 4-12% Bis-Tris Plus Gel	Thermo Fisher Scientific	Cat#NW04120BOX
Deposited Data		
Affymetrix	This paper	E-MTAB-6783; E-MTAB-7782
m^6A meRIP-Seq datasets	This paper	E-MTAB-6791; E-MTAB-7783
RIBO-seq	This paper	E-MTAB-7785
SLAM-seq	This paper	E-MTAB-7784
Experimental Models: Cell Lines		
THP-1	ATCC	Cat#TIB-202
NOMO-1	DSMZ	Cat#ACC 542
Experimental Models: Organisms/Strains		
Ythdf2$^{fl/fl}$ mice	Ivanova et al., 2017	N/A
Vav-iCre mice	The Jackson Laboratory	Stock No: 008610
Mx1-Cre mice	The Jackson Laboratory	Stock No: 003556
NOD *scid* gamma	The Jackson Laboratory	Stock No: 005557
Oligonucleotides		
HPRT1 Taqman Gene Expression Assays	ThermoFisher Scientific	Cat#Hs02800695_m1
YTHDF2 Taqman Gene Expression Assays	ThermoFisher Scientific	Cat#Hs00212357_m1
shRNA KD1, 5′-TACTGATTAAGTCAGGATTAA-3′	Sigma-Aldrich	Cat#TRCN0000254410
shRNA KD2, 5′- CGGTCCATTAATAACTATAAC −3′	Sigma-Aldrich	Cat#TRCN0000254336
shRNA CTL, 5′-TTCTCCGAACGTGTCACGTT-3′	Custom cloned pLKO.1-puro	N/A

(*Continued on next page*)

Continued

REAGENT or RESOURCE	SOURCE	IDENTIFIER
Software and Algorithms		
Bioconductor Limma Package	Ritchie et al., 2015	https://bioconductor.org/packages/release/bioc/html/limma.html
Bioconductor topGO package	Bioconductor	https://bioconductor.org/packages/release/bioc/html/topGO.html
Bioconductor Simpleaffy package	Wilson and Miller, 2005	https://bioconductor.org/packages/release/bioc/html/simpleaffy.html
Bioconductor arrayQualityMetrics package	Kauffmann et al., 2009	http://bioconductor.org/packages/release/bioc/html/arrayQualityMetrics.html
deepTools package	Ramírez et al., 2014	https://deeptools.readthedocs.io/en/develop/
ConsensusPathDB (CPDB) software.	Kamburov et al., 2013	http://cpdb.molgen.mpg.de/
Bioconductor GVIZ package	Hahne and Ivanek, 2016	https://bioconductor.org/packages/release/bioc/html/Gviz.html
stats R package	R project	http://www.R-project.org/
GraphPad Prism 6 software	GraphPad Software, Inc.	N/A
HISAT2	Kim et al., 2015	https://ccb.jhu.edu/software/hisat2/index.shtml
MACS2	Zhang et al., 2008	https://github.com/taoliu/MACS
HOMER		http://homer.ucsd.edu/homer/motif/
BEDtools	Quinlan and Hall, 2010	https://bedtools.readthedocs.io/en/latest/
SlamDunk		https://github.com/t-neumann/slamdunk
Kallisto	Bray et al., 2016	https://pachterlab.github.io/kallisto/
Xtail	Xiao et al., 2016b	https://github.com/xryanglab/xtail
DESeq2	Love et al., 2014	https://bioconductor.org/packages/release/bioc/html/DESeq2.html
RMAexpress software		http://rmaexpress.bmbolstad.com/
Other		
MethoCultTM M3434	STEMCELL Technologies	Cat#M3434
MethoCultTM M3231	STEMCELL Technologies	Cat#M3231

CONTACT FOR REAGENT AND RESOURCE SHARING

Further information and requests for reagents may be directed to, and will be fulfilled by the Lead Contact, Kamil Kranc (kamil.kranc@qmul.ac.uk).

EXPERIMENTAL MODEL AND SUBJECT DETAILS

Mice

All experiments on animals were performed under UK Home Office authorisation. All mice were on the C57BL/6 genetic background. *Ythdf2*$^{fl/fl}$ mice were described previously (Ivanova et al., 2017). *Vav-iCre* (de Boer et al., 2003), *Mx1-Cre* (Kühn et al., 1995), and NOD *scid* gamma mice were purchased from the Jackson Laboratory. All transgenic and knockout mice were CD45.2^{+}. Congenic recipient mice were CD45.1^{+}/CD45.2^{+}.

Human tissue & ethical approvals

Use of human tissue was in compliance with the ethical and legal framework of the United Kingdom's Human Tissue Act, 2004. Primary human AML samples were from Manchester Cancer Research Centre's Tissue Biobank (instituted with approval of the South Manchester Research Ethics Committee). Their use was authorized following ethical review by the Tissue Biobank's scientific sub-committee, and with the informed consent of the donor. Normal CD34^{+} HSPCs surplus to requirements were from patients undergoing autologous transplantation for lymphoma or myeloma. Their use was authorized by the Salford and Trafford Research Ethics Committee and, for samples collected since 2006, following the written informed consent of donors.

METHOD DETAILS

Flow cytometry

All BM and FL cells were prepared and analyzed as described previously (Guitart et al., 2017; Guitart et al., 2013; Kranc et al., 2009; Mortensen et al., 2011; Vukovic et al., 2016). BM cells were isolated by crushing tibias and femurs using a pestle and mortar. FL cells were prepared by mashing the tissue and passing through a 70μm strainer. Single cell suspensions from BM, FL or PB were incubated with Fc block and then stained with antibodies. For HSC and progenitor cell analyses, following incubation with Fc block, unfractionated BM cells were stained with lineage markers containing biotin-conjugated anti-CD4, anti-CD5, anti-CD8a, anti-CD11b, anti-B220, anti-Gr-1 and anti-Ter119 antibodies together with APC-Cy7-conjugated anti-c-Kit, Pacific Blue-conjugated anti-Sca-1, PE-conjugated anti-CD48 and PE-Cy7-conjugated anti-CD150 antibodies. Biotin-conjugated antibodies were then stained with PerCP-conjugated streptavidin. For analyses of differentiated cells, following incubation with Fc block, spleen or BM cell suspensions were stained with PerCP-conjugated anti-B220 and APC-Cy7-conjugated anti-CD19 antibodies for B cells; Pacific Blue-conjugated anti-CD11b and PE-Cy7-conjugated anti-Gr-1 for myeloid cells; APC-conjugated anti-CD8 antibodies and PE-conjugated anti-CD4 antibodies for T cells.

To distinguish $CD45.2^+$-donor derived cells in PB or BM of transplanted mice, BV711-conjugated anti-CD45.1 and Pacific Blue-conjugated anti-CD45.2 antibodies were used. For HSC and progenitor staining in transplanted mice, APC-conjugated anti-c-Kit, and APC-Cy7-conjugated anti-Sca-1 were used; the remainder of the staining was as described above. For analyses of differentiated cells in BM of transplanted mice, myeloid cells were stained with PE-conjugated anti-CD11b, PE-Cy7-conjugated anti-Gr-1 and APC-conjugated anti-Ter119 for erythroid cells. Lymphoid cells were stained separately, as described above. PB of transplanted mice was stained with BV711-conjugated anti-CD45.1, Pacific Blue-conjugated anti-CD45.2, PE-conjugated anti-CD4 and-CD8a, PE-Cy7-conjugated anti-Gr-1, APC-conjugated anti-CD11b, and APC-Cy7-conjugated anti-CD19. TO-PRO-3 or DAPI were used for dead cell exclusion.

Flow cytometry analyses were performed using a LSRFortessa (BD). Cell sorting was performed on a FACSAria Fusion (BD).

Colony forming cells (CFC) assays

CFC assays were carried out using MethoCultTM M3434 (STEMCELL Technologies) methylcellulose medium. Two technical replicates were used per each biological replicate in each experiment. Colonies were tallied at day 10. Human primary AML samples were enumerated after 7 days of culture in semisolid medium in the presence of recombinant IL-6, G-CSF and TPO (20ng/ml) using puromycin as the selectable marker.

Leukemic transformation

$c\text{-}Kit^+$ cells were prepared from FLs of 14.5 dpc embryos using c-Kit (CD117) enrichment with MACS columns (Miltenyi Biotec). 200,000 $c\text{-}Kit^+$ cells were co-transduced with MSCV-Meis1a-puro and MSCV-Hoxa9-neo retroviruses. Transduced cells were subjected to three rounds of CFC assays in MethoCultTM M3231 (STEMCELL Technologies) supplemented with 20ng/ml SCF, 10ng/ml IL-3, 10ng/ml IL-6 and 10ng/ml GM-S*CF.* Colonies were counted 5 days after plating, and 2,000 cells were re-plated.

Syngeneic transplantation assays

$CD45.1^+/CD45.2^+$ recipient mice were lethally irradiated using a split dose of 11 Gy (two doses of 5.5 Gy administered at least 4 hours apart) at an average rate of 0.58 Gy/min using a Cesium 137 GammaCell 40 irradiator.

For primary transplantations 200 $LSKCD48^-CD150^+$ HSCs (per recipient) sorted from BM of the donor mice were mixed with 200,000 support $CD45.1^+$ BM cells and transferred into lethally irradiated $CD45.1^+/CD45.2^+$ recipients. For secondary transplantations 2,000-3,000 $CD45.2^+$ LSK cells sorted from BM of primary recipients were mixed with 200,000 support $CD45.1^+$ wild-type BM cells and re-transplanted. All recipient mice were culled and analyzed 16-20 weeks post-transplantation.

For transplantations of leukemic cells, 50,000-100,000 *Meis1/Hoxa9*-transduced $c\text{-}Kit^+$ cells were transplanted into lethally irradiated $CD45.1^+/CD45.2^+$ recipient mice (together with 200,000 unfractionated support $CD45.1^+$ wild-type BM cells). For secondary transplantation, 10,000 $CD45.2^+c\text{-}Kit^+$ cells sorted from BM of primary recipients were transplanted into lethally irradiated secondary $CD45.1^+/CD45.2^+$ recipient mice (together with 200,000 unfractionated support $CD45.1^+$ wild-type BM cells).

Xenotransplantation experiments

THP-1 cells transduced with CTL or KD lentiviruses were tail vein injected into non-irradiated 12 week-old female non-obese diabetic (NOD)/LtSz-severe combined immune-deficiency (SCID) IL-$2R\gamma c^{null}$ (NSG) mice ($1x10^6$ cells per 200 μL per mouse). Mice were killed one month after transplantation. For survival curve analyses, 10,000 or 1,000 cells per NSG mouse were injected. To assess human AML burden, cells were stained with anti-human PE-conjugated anti-CD45 and APC-conjugated anti-CD33.

pIpC administration

Mice were injected intraperitoneally every other day with 300 μg pIpC (GE Healthcare) for a total of 6 doses, as previously described (Guitart et al., 2017; Guitart et al., 2013; Kranc et al., 2009).

shRNA-mediated YTHDF2 knockdown

THP-1 cells were transduced with lentiviruses expressing shRNAs (shRNA KD1, 5′-TACTGATTAAGTCAGGATTAA-3′ [TRCN0000254410, Sigma-Aldrich]; shRNA KD2, 5′- CGGTCCATTAATAACTATAAC −3′ [TRCN0000254336, Sigma-Aldrich]; and shRNA CTL, 5′-TTCTCCGAACGTGTCACGTT-3′; GE Healthcare). Selection of efficiently transduced cells was achieved by treatment with puromycin (2 μg/mL final concentration).

Cell proliferation, cell death and cell differentiation analyses

Lentivirus-transduced THP-1 were seeded at $15x10^4$/mL after puromycin selection. Viable cells were counted by trypan blue exclusion at the indicated time points. To analyze cells undergoing apoptosis, cells were suspended in binding buffer containing Annexin V-PE and DAPI. To assess myeloid differentiation, cells were stained with PE-conjugated anti-CD14 and APC-conjugated anti-CD11b antibodies.

Primary human AML patient derived samples

For western blotting shown in Figure 1B, the following samples were used: 70 (karyotype 46,XY,del(7)(q22q32)[20]), 104 (karyotype 46,XX,t(6;9;11)(p2?1;p22;q23)[6]/45,idem,der(15)t(15;17)(p11.2;q11.2),-17[4] [variant of t(9;11)]0, 108 (karyotype 46,XX,t(6;11)(q27;q23)[10]), 149 (karyotype 46,XX,t(15;17)(q22;q11.2)[7]/46,sl,-6,add(16)(q12),+mar[3]/46,XX[3]), 163 (karyotype 45,X,-Y,t(8;21)(q22;q22)[8]/46,XY[2]), 191 (karyotype 46,XX [20]), 205 (karyotype 44,XX,add(3)(p25),-5,-7[12]), 419 (karyotype 46,XX,t(1;22)(p21;p11.2),ins(10;11)(p12;q23q1?4)[10] nb variant of t(10;11) MLL-MLLT10 fusion), 539 (karyotype 46,XY [20]), 685 (karyotype 46,XX,t(6;9)).

For CFC assays shown in Figures 2L and 2M, the following samples were used: 160 (AML1) (karyotype 46,XX,t(9;11)(p22;q23),der(21;22)(q10;q10),+der(21;22)[cp10]; MLL-MLLT3 rearrangement; clonal evolution with add(Xp); add(4q); add(7q); +21 at relapse), 292 (AML2) (karyotype 46,XX,t(15;17); PML-RARA rearrangement [no cyto report available]), 251 (AML3) (karyotype 46,XY,t(6;9)(p22;q34)[9]/46,XY,der(6)t(6;9),der(9)t(6;9)del(9)(q21q34)[2]).

Western blotting

Proteins extracted from CTL, KD1 and KD2 THP-1 cells were subjected to SDS–PAGE (Bolt 4%–12% Bis-Tris Plus Gel, ThermoFisher Scientific, NW04120BOX) and then transferred onto a polyvinylidene fluoride membranes. Membranes were blocked in 10% milk-PBST (PBS with 0.1% Tween20) and probed with anti-YTHDF2 (1:5000, ON at 4°C) and anti- Histone3 (1:5000, 1h at room temperature). After incubation with appropriate horseradish peroxidase-coupled secondary antibody, proteins were detected with SuperSignal West Dura Extended Duration Substrate (ThermoFisher Scientific, 34075) and acquired on the Amersham Imager 600 (GE Healthcare life Sciences).

Affymetrix

RNA extraction from *Meis1/Hoxa9*-transduced c-Kit$^+$ cells was performed using TRIzol (Thermo Fisher Scientific). Total RNA was used to synthesize Biotinylated cDNA with the Ambion WT Expression kit (Ambion, 4491974). cDNA was fragmented and labeled with the Affymetrix, WT Terminal and Control Kits (Affymetrix, 901524) and then hybridized for 16 hours at 45°C on a GeneChip Mouse Gene 2.0 ST Array. The chip was later washed and stained with the Affymetrix Fluidics Station 450. Data were processed and analyzed using the Bioconductor Limma Package (Ritchie et al., 2015). Samples were normalized using the rma function and differential expression was assessed using linear modeling. Log2-fold-changes and moderated t-statistics were calculated using the contrasts.fit function. To determine the gene ontology (GO) enrichment of differentially expressed genes, we used the topGO R package. Fisher's exact test was used to assess enrichment for the biological process ontology.

Analyses of YTHDF2 expression in human AML samples

To generate Figure 1A the following publicly available datasets were used: GSE10358, GSE52891, GSE61804, GSE68833, GSE12417, GSE13159, GSE15061, GSE15434, GSE16015, GSE19577, and GSE22845 (Bachas et al., 2015; Haferlach et al., 2009, 2010; Klein et al., 2009; Metzeler et al., 2008; Metzelder et al., 2015; Mills et al., 2009; Pigazzi et al., 2011; Taskesen et al., 2011; Tomasson et al., 2008). Exclusion criteria included datasets with less than 20 samples, samples with undefined tissue of origin, cell type and karyotype, in addition to RAEB samples. Only BM samples, with a total of 1732 samples were retained for further analysis. The Simpleaffy package from Bioconductor was used to extract quality measurement of microarrays (Gentleman et al., 2004; Wilson and Miller, 2005). RNA degradation was assessed based on 3′ to 5′ ratio of *GAPDH* and *ACTNB* genes. Samples with NUSE < 1.05 and relative log expression (RLE) < 0.15 were excluded from further analysis (McCall et al., 2011). The retained samples were assessed for their homogeneity using the Bioconductor arrayQualityMetrics package (Kauffmann et al., 2009). Low quality RNA and outlier samples were excluded, while high quality samples retained after quality control were background corrected and normalized using RMAexpress software (http://rmaexpress.bmbolstad.com/). Pairwise comparisons between each karyotype and control were performed using Student's t test.

m^{6}A meRIP-Seq

m^{6}A meRIP-Seq library preparation was performed as previously described (Lin et al., 2016) from *Ythdf2*^{CTL} pre-leukemic cells. Three biological replicates for each condition were used. Reads were aligned to the mouse or human reference genome using HISAT2 (Kim

et al., 2015) and peaks were called using MACS2 (Zhang et al., 2008). To analyze the distribution of peaks along the transcripts, bedgraph files were converted to bigWig format and used as input for the computeMatrix function of the deepTools package (Ramírez et al., 2014). Motif enrichment was done using HOMER selecting a motif length of 6 nucleotides. Background regions were generated by shuffling peaks along the transcriptome using the shuffleBed tool from the BEDtools suite (Quinlan and Hall, 2010). Network analysis was performed using the ConsensusPathDB (CPDB) software (Kamburov et al., 2013). For gene set enrichment analysis (GSEA), the GSE76008 dataset (Ng et al., 2016) was used to rank genes according to the engraftment potential of pre-leukemic cells. The GVIZ bioconductor package was used for peak visualization (Hahne and Ivanek, 2016).

Correlation with YTHDF2 was measured to determine robust YTHDF2 targets after the knockout (Månsson et al., 2004). Briefly, Pearson correlation between YTHDF2 and the identified YTHDF2 targets was calculated using the 1732 AML samples previously described. Correlation significance was measured using parametric test with length (genes)-2 degrees of freedom (cor.test function, stats package, R project, http://www.R-project.org/), and adjusted for multiple comparisons using Benjamini & Hochberg method (Benjamini and Hochberg, 1995). Genes with negative coefficients and adjusted p value < 0.05 were considered strong targets of YTHDF2.

SLAM-seq

SLAM-seq libraries were prepared using the Lexogen catabolic kit (cat. no. 062.24) and the Lexogen QuantSeq 3′ mRNA-Seq Library Prep Kit FWD for Illumina (cat. no. 015.24) in both cases following manufacturers' instructions. S4U was used at 2.9 μM, as determined by the cell viability titration assay. Medium with 4SU was used for pre-leukemic cells labeling for 12 hours and was later replaced with 4SU-free medium (time 0). Cells were collected immediately after medium change and at 1, 3, and 9 hours. Libraries were sequenced using an Illumina HiSeq platform in a 50 bp single-end mode. Biological triplicates for both *Ythdf2*^{CTL} and *Ythdf2*^{cKO} pre-leukemic cells were used to generate the different libraries sets. SLAM-seq libraries were analyzed as previously described (Herzog et al., 2017). Briefly, T to C conversion rates were obtained using the SlamDunk pipeline. Conversion rates across different time points were normalized to time 0 for each gene and were used to fit a first order decay reaction with the R stats package nls function.

RIBO-seq

RIBO-seq libraries were prepared as previously described (Reid et al., 2015). Briefly, pre-leukemic cells were lysed with $CaCl_2$ 4 mM, MgCl 10 mM, K-HEPES pH 7.2 25 mM, KOAc 200 mM and NP-40 1%. The lysate was cleared from cell debris, diluted 1:1 in water, and digested with MNase 10 μg/ml for 30 minutes at 37°C. Digested RNA was extracted with QIAzol and later treated with PNK (NEB) for 30 minutes at 37°C. To isolate ribosome-protected mRNA fragments (RPFs), the PNK-treated RNA was resolved on a 15% Novex TBE-Urea Gel (EC6885BOX), and RPFs 25 to 40 nucleotides long were excised and purified. Libraries were then prepared using the NEBNext® Multiplex Small RNA Library Prep Set for Illumina following manufacturer's instructions. For input controls, total RNA was extracted from the pre-leukemic cell lysates before MNase digestion using QIAzol. Samples were then depleted of ribosomal RNA using the Epicenter Ribo-zero kit (cat. no. MRZH116), and libraries were generated using the SENSE Total RNA-Seq Library Prep Kit (cat no. 009.08) following manufacturer's instructions. Libraries were sequenced with the Illumina HiSeq platform in a 50 bp single-end mode. Biological triplicates were used to generate libraries for both *Ythdf2*^{CTL} and *Ythdf2*^{cKO} pre-leukemic cells. For the RIBO-seq analysis, we used Kallisto (Bray et al., 2016) to obtain read counts per gene for the RPF and mRNA libraries. Read counts were then used to calculate the differential translational efficiency between *Ythdf2*^{CTL} and *Ythdf2*^{cKO} pre-leukemic cells with Xtail (Xiao et al., 2016b). To estimate the relative translational efficiency for genes in each condition, we compared RPF and mRNA read counts using DESeq2 (Love et al., 2014).

DATA AND SOFTWARE AVAILABILITY

Accession

Affymetrix, m^{6}A meRIP-Seq, RIBO-seq and SLAM-seq datasets were deposited in ArrayExpress under the following accession numbers: E-MTAB-6783, E-MTAB-7782, E-MTAB-6791, E-MTAB-7783, E-MTAB-7785 and E-MTAB-7784. Data from NOMO-1 and MA9.3ITD human cell lines were obtained from previously published work (Su et al., 2018) through the following accession number: GSE87190.

QUANTIFICATION AND STATISTICAL ANALYSIS

Statistical analyses were performed using GraphPad Prism 6 software (GraphPad Software, Inc.). P values were calculated using a two-tailed Mann–Whitney U test unless stated otherwise. Kaplan-Meier survival curve statistics were determined using the Log-rank (Mantel Cox) test.

Cell Stem Cell, Volume *25*

Supplemental Information

Targeting the RNA m^{6}A Reader YTHDF2 Selectively Compromises Cancer Stem Cells in Acute Myeloid Leukemia

Jasmin Paris, Marcos Morgan, Joana Campos, Gary J. Spencer, Alena Shmakova, Ivayla Ivanova, Christopher Mapperley, Hannah Lawson, David A. Wotherspoon, Catarina Sepulveda, Milica Vukovic, Lewis Allen, Annika Sarapuu, Andrea Tavosanis, Amelie V. Guitart, Arnaud Villacreces, Christian Much, Junho Choe, Ali Azar, Louie N. van de Lagemaat, Douglas Vernimmen, Ali Nehme, Frederic Mazurier, Tim C.P. Somervaille, Richard I. Gregory, Dónal O'Carroll, and Kamil R. Kranc

Supplemental Information

Targeting the RNA m^{6}A reader YTHDF2 selectively compromises cancer stem cells in acute myeloid leukemia

Jasmin Paris, Marcos Morgan, Joana Campos, Gary J. Spencer, Alena Shmakova, Ivayla Ivanova, Christopher Mapperley, Hannah Lawson, David A. Wotherspoon, Catarina Sepulveda, Milica Vukovic, Lewis Allen, Annika Sarapuu, Andrea Tavosanis, Amelie V. Guitart, Arnaud Villacreces, Christian Much, Junho Choe, Ali Azar, Louie N. van de Lagemaat, Douglas Vernimmen, Ali Nehme, Frederic Mazurier, Tim C.P. Somervaille, Richard I Gregory, Dónal O'Carroll & Kamil R. Kranc

SUPPLEMENTARY INFORMATION

Figure S1, related to Figures 1 and 2
Figure S2, related to Figure 3
Figure S3, related to Figure 4
Table S1, related to Figure 3

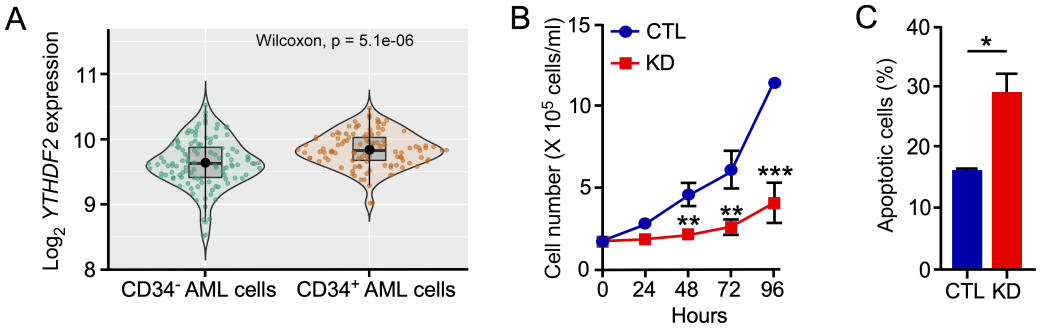

Figure S1, related to Figures 1 and 2: The requirement for YTHDF2 in human AML
(**A**) *YTHDF2* gene expression in CD34$^-$ and CD34$^+$ AML cell compartments. This figure was generated by reanalysis of the dataset published by Ng S., et al., Nature *540*, 433-437, 2016. (**B**) Proliferation assays with NOMO-1 cells expressing CTL and KD shRNAs. Mean ± s.e.m., n = 3. **, P < 0.01; ***, P < 0.001. (**C**) Apoptosis assays. Data are mean ± s.e.m., n = 3. *, P < 0.05.

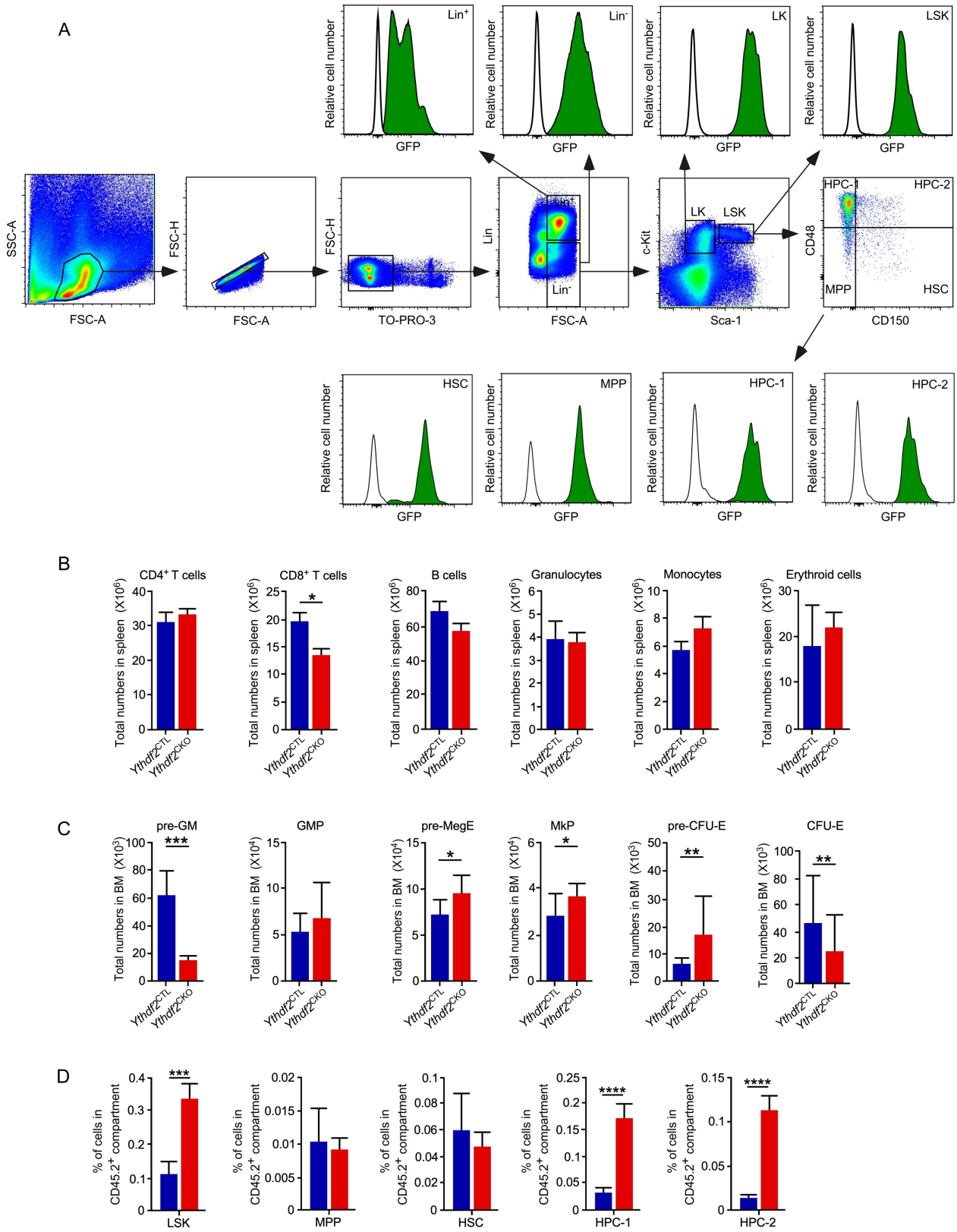
A
Lin+
Lin-
LK
LSK
Relative cell number
GFP
SSC-A
FSC-A
FSC-H
TO-PRO-3
Lin
c-Kit
Sca-1
CD48
CD150
HPC-1
HPC-2
HSC
MPP
B
CD4+ T cells
CD8+ T cells
B cells
Granulocytes
Monocytes
Erythroid cells
Total numbers in spleen (X10^6)
YthdfCTL
YthdfCKO
C
pre-GM
GMP
pre-MegE
MkP
pre-CFU-E
CFU-E
Total numbers in BM (X10^3)
Total numbers in BM (X10^4)
D
% of cells in CD45.2+ compartment
LSK
MPP
HSC
HPC-1
HPC-2

Figure S2, related to Figure 3: YTHDF2 expression at different levels of hematopoietic hierarchy and phenotypes resulting from hematopoiesis-specific *Ythdf2* deletion. (**A**) Total BM cells from *Ythdf2*^{CTL} and wild-type mice were first live and size gated using forward scatter area (FSC-A) and side scatter area (SSC-A). Doublets were excluded using FSC-A versus FSC height (FSC-H). Lineage positive (Lin^+) and Lin^- were separated. Lin^- cells contains the LK and LSK cells. LSK cells were further sub-gated on HSC, MPP, HPC-1, and HPC-2 fractions. GFP expression is shown in each population (green histograms). White histograms indicate the lack of GFP expression in wild-type control cells. (**B**) Total numbers of T cells, B cells, granulocytes, monocytes and erythroid cells in spleens from *Ythdf2*^{CTL} and *Ythdf2*^{CKO} mice. Data are mean ± s.e.m. (*n* = 5-6 mice per genotype). *, P < 0.05. (**C**) Total numbers of committed progenitor cells in the BM of *Ythdf2*^{CTL} and *Ythdf2*^{CKO} mice. Data are mean ± s.e.m. (*n* = 5-6 mice per genotype). *, P<0.05; **, P<0.01; ***, P<0.001. (**D**) Percentage of LSK, HSC, MPP, HPC-1 and HPC-2 populations within the donor-derived $CD45.2^+$ compartment of the recipient mice shown in Figure 3L. Data are mean ± s.e.m. (*n* = 6-9 recipients per genotype), ***, P < 0.001; ****, P < 0.0001.

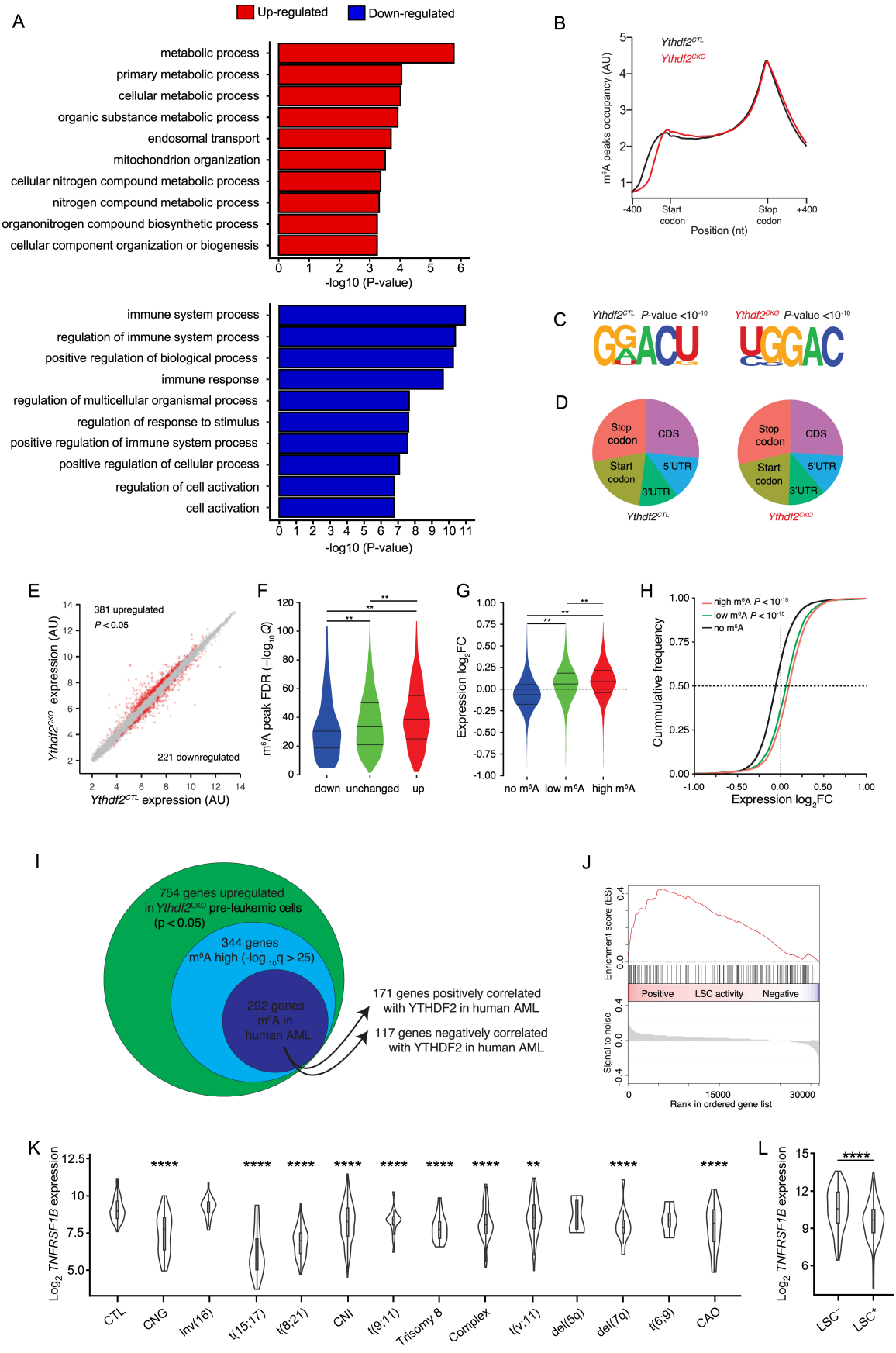
A
Up-regulated
Down-regulated
metabolic process
primary metabolic process
cellular metabolic process
organic substance metabolic process
endosomal transport
mitochondrion organization
cellular nitrogen compound metabolic process
nitrogen compound metabolic process
organonitrogen compound biosynthetic process
cellular component organization or biogenesis
-log10 (P-value)
immune system process
regulation of immune system process
positive regulation of biological process
immune response
regulation of multicellular organismal process
regulation of response to stimulus
positive regulation of immune system process
positive regulation of cellular process
regulation of cell activation
cell activation
-log10 (P-value)
B
Ythdf2CTL
Ythdf2CKO
m6A peaks occupancy (AU)
-400
Start codon
Stop codon
+400
Position (nt)
C
Ythdf2CTL P-value <10-10
Ythdf2CKO P-value <10-10
D
Stop codon
CDS
Start codon
5'UTR
3'UTR
Ythdf2CTL
Ythdf2CKO
E
381 upregulated
P < 0.05
221 downregulated
Ythdf2CKO expression (AU)
Ythdf2CTL expression (AU)
F
m6A peak FDR (−log10Q)
down
unchanged
up
G
Expression log2FC
no m6A
low m6A
high m6A
H
high m6A P < 10-15
low m6A P < 10-15
no m6A
Cummulative frequency
Expression log2FC
I
754 genes upregulated in Ythdf2CKO pre-leukemic cells (p < 0.05)
344 genes m6A high (-log10q > 25)
292 genes m6A in human AML
171 genes positively correlated with YTHDF2 in human AML
117 genes negatively correlated with YTHDF2 in human AML
J
Enrichment score (ES)
Positive
LSC activity
Negative
Signal to noise
Rank in ordered gene list
K
Log2 TNFRSF1B expression
CTL
CNG
inv(16)
t(15;17)
t(8;21)
CN
t(9;11)
Trisomy 8
Complex
t(v;11)
del(5q)
del(7q)
t(6;9)
CAO
L
Log2 TNFRSF1B expression
LSC-
LSC+

Figure S3, related to Figure 4: YTHDF2 regulates the leukemic and pre-leukemic cell transcriptomes. (A) Gene ontology analysis for the upregulated and downregulated genes in *Ythdf2*^{CKO} pre-leukemic cells. The enrichment is presented as –log10 (p-value). **(B)** m^{6}A peak occupancy along a transcript body model are shown for *Ythdf2*^{CTL} (black) and *Ythdf2*^{CKO} (red) pre-leukemic cells. One representative sample of three biological replicates is shown for each genotype. Transcripts models were extended 400 nucleotides upstream and downstream of the start and stop codons, respectively. **(C)** m^{6}A-seq motif enrichments and associated *P*-values are shown for each genotype. **(D)** m^{6}A peak overlaps with different transcript regions (5'UTR; start codon; coding sequence, CDS; stop codon; 3'UTR) are shown for each condition. **(E)** Transcript expression scatter plot from *Ythdf2*^{CTL} and *Ythdf2*^{CKO} leukemic cells. Significantly upregulated or downregulated transcripts are highlighted in red (Adjusted moderate t-student test, $P < 0.05$). Four biological replicates were used for each condition. **(F)** m^{6}A peak FDR (-log$_{10}$Q) in pre-leukemic cells for transcripts grouped according to expression changes between *Ythdf2*^{CTL} and *Ythdf2*^{CKO} leukemic cells is shown (down, genes significantly downregulated in *Ythdf2*^{CKO} ($P < 0.05$); unchanged, genes not significantly changing in *Ythdf2*^{CKO}; up, genes significantly upregulated in *Ythdf2*^{CKO} ($P < 0.05$). (** indicates $P < 0.01$, Mann-Whitney, two-sided test). The upper and lower quartiles and the median are shown for each group. **(G)** Violin plots showing expression change between *Ythdf2*^{CTL} and *Ythdf2*^{CKO} leukemic cells for pre-leukemic cells not methylated (no m^{6}A), methylated (m^{6}A, -log$_{10}$Q ≤ 25) and highly methylated (m^{6}A high, -log$_{10}$Q > 25) transcripts (** indicates $P < 0.01$, Mann-Whitney, two-sided test). The upper and lower quartiles and the median are shown for each group. **(H)** Cumulative distribution of transcripts' expression change in *Ythdf2*^{CTL} and *Ythdf2*^{CKO} pre-leukemic cells for not methylated, methylated and highly methylated transcripts as in **G**. **(I)** Overview of gene selection criteria for this study. Upregulated genes in *Ythdf2*^{CKO} pre-leukemic cells, highly methylated in *Ythdf2*^{CTL} pre-leukemic cells and methylated in human MA9.3ITD and NOMO-1 cells were further divided between genes positively or negatively correlated with YTHDF2 across more than 1732 human AML samples. (**J**) GSEA of genes positively correlated with YTHDF2 as defined in **I** using the LSC signature (Ng et al., 2016) gene set is shown. **(K)** *TNFRSF1B* gene expression in control (CTL) and different cytogenetic subgroups of human AML bone marrow samples. Violin plots show the distribution of log$_2$ expression values. Horizontal line in the boxplots indicates median. **, P<0.01; ****, P<0.0001. CNG, cytologically normal with good prognosis; CNI, cytologically normal with intermediate prognosis; CAO, cytologically abnormal not otherwise specified. **(L)** *TNFRSF1B* gene expression in primitive AML cell compartments with (LSC$^+$) and without (LSC$^-$) leukemic engraftment potential. ****, P<0.0001.

	Ythdf2^{CTL}	*Ythdf2*^{iCKO}	P value
WBC (/μl)	5883 ± 1135	8133 ± 1114	0.258
RBC (X10^4/μl)	825 ± 99.8	889 ± 73.8	0.699
Hb (g/dl)	14.02 ± 0.9	13 ± 0.95	0.563
PLT (X10^4/μl)	58.57 ± 7.96	92.5 ± 12.8	0.132
CD4$^+$ T cells (/μl)	1094 ± 206	1489 ± 128.5	0.179
CD8$^+$ T cells (/μl)	929.3 ± 178.7	1093 ± 103.2	0.699
B cells (/μl)	2385 ± 494.5	2784 ± 374.1	0.588
Granulocytes (/μl)	902 ± 312.6	1378 ± 315.7	0.24
Monocytes (/μl)	310.4 ± 58.38	563.4 ± 92.13	0.065

Table S1, related to Figure 3: Peripheral blood counts of *Ythdf2*^{CTL} and *Ythdf2*^{iCKO} mice 4 weeks after last pIpC injections. Data are mean ± s.e.m. (*n* = 6 mice per genotype). P values are indicated.